AUTONOMOUS UNIVERSITY OF BAJA CALIFORNIA

Faculty of Engineering, Architecture and Design

Master and Doctorate in Sciences and Engineering

Design and construction of an electrical impedance tomography system using a single board computer

Thesis

for obtaining the degree of

Doctor in Sciences

that presents:

Francisco Zamora Arellano

Thesis supervisors

Dr. Everardo Inzunza Gonzalez **Dr. Oscar Roberto López Bonilla**

Ensenada, Baja California, Mexico, January, 2021.

AUTONOMOUS UNIVERSITY OF BAJA CALIFORNIA

Faculty of Engineering, Architecture and Design

Master and Doctorate in Sciences and Engineering

Design and construction of an electrical impedance tomography system, using a single board computer

Thesis

for obtaining the degree of

Doctor in Sciences

that presents:

FRANCISCO ZAMORA ARELLANO

and approved by the committee:

Dr. Everardo Inzunza Gonzalez
Thesis supervisor

Dr. Oscar Roberto López Bonilla
Thesis supervisor

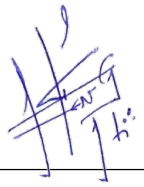

Dr. Enrique Efrén García Guerrero
Committee member

Dra. Almendra Villela y Mendoza
Committee member

Dr. Jesús Everardo Olguín Tiznado
Committee member

Ensenada, Baja California, Mexico, December 2020.

RESUMEN de la tesis de **Francisco Zamora Arellano**, presentada como requisito para obtener el grado de **DOCTOR en CIENCIAS**, del programa de Maestría y Doctorado en Ciencias e Ingeniería de la Universidad Autónoma de Baja California. Ensenada, Baja California México, December 2020.

Diseño y construcción de un sistema de tomografía por impedancia eléctrica, usando una computadora de placa sencilla

Resumen aprobado por:

Dr. Everardo Inzunza Gonzalez
Director de tesis

Dr. Oscar Roberto López Bonilla
Co-Director de tesis

La tomografía de impedancia eléctrica (EIT por sus siglas en inglés) es un procedimiento útil con aplicaciones en la industria y la medicina, particularmente en el área de los pulmones y el cerebro. En esta tesis doctoral, se presenta el desarrollo de un sistema EIT portátil, confiable y de bajo costo para la reconstrucción de imágenes mediante el uso de un computadora de placa sencilla (SBC por sus siglas en inglés). La novedad de esta tesis doctoral es el completo desarrollo de hardware de un sistema de tomografia por impedancia eléctrica, ademas de tres algoritmos simples y eficientes que se pueden implementar en SBC. El sistema EIT propuesto aplica el método de voltaje adyacente, comenzando con una etapa de adquisición de impedancias que envía datos a una Raspberry Pi 4 (RPi4) como SBC. Para realizar la reconstrucción de la imagen, se desarrolló una interfaz de usuario utilizando GNU Octave para RPi4 y la biblioteca EIDORS. Se realiza un análisis estadístico para determinar el mejor valor promedio de las muestras medidas mediante el uso de un convertidor analógico a digital (ADC por sus siglas en inglés) con una capacidad de 30 kSPS y una resolución de 24 bit. Las pruebas para el sistema EIT propuesto se realizaron utilizando materiales como metal, vidrio y una naranja para simular su aplicación en la industria alimentaria. Los resultados experimentales muestran que la mediana estadística es más precisa con respecto a la medida de voltaje real, sin embargo, representa un mayor costo computacional, por lo que la media se calcula y se mejora descartando los valores de los datos en un estado transitorio, logrando mayor precisión que la mediana para determinar el valor de voltaje real, mejorando la calidad de las imágenes reconstruidas. Se presenta una comparación de rendimiento entre una computadora personal (PC por sus siglas en inglés) y RPi4. El sistema EIT propuesto ofrece una excelente relación costo-beneficio con respecto a un PC tradicional, teniendo en cuenta precisión, exactitud, consumo de energía, precio, peso ligero, tamaño, portabilidad y confiabilidad. El sistema EIT propuesto tiene una aplicación potencial en la ventilación mecánica, la industria alimentaria y el monitoreo de la salud estructural.

Palabras clave: Tomografía de impedancia eléctrica; EIT; reconstrucción de imagenes; computadora de placa sencilla; Raspberry Pi 4; instrumentación electrónica.

Thesis **ABSTRACT** of **Francisco Zamora Arellano**, presented as requirement to obtain the degree of **DOCTOR in SCIENCES**, from the program of Master and Doctorate in Sciences and Engineering of Autonomous University of Baja California. Ensenada, Baja California México, December 2020.

Design and construction of an electrical impedance tomography system, using a single board computer

Abstract approved by:

Dr. Everardo Inzunza Gonzalez
Thesis supervisor

Dr. Oscar Roberto López Bonilla
Thesis supervisor

Electrical impedance tomography (EIT) is a useful procedure with applications in industry and medicine, particularly in the lungs and brain area. In this Ph.D. thesis, the development of a portable, reliable and low-cost EIT system for image reconstruction by using a single board computer (SBC) is introduced herein. The novelty of this Ph.D. thesis is the hardware development of a complete low-cost EIT system, as well as three simple and efficient algorithms that can be implemented on SBC. The proposed EIT system applies the adjacent voltage method, starting with an impedance acquisition stage that sends data to a Raspberry Pi 4 (RPi4) as SBC. To perform the image reconstruction, a user interface was developed by using GNU Octave for RPi4 and the EIDORS library. A statistical analysis is performed to determine the best average value from the samples measured by using an analog-to-digital converter (ADC) with a capacity of 30 kSPS and 24-bit resolution. The tests for the proposed EIT system were performed using materials such as metal, glass, and an orange to simulate its application in food industry. Experimental results show that the statistical median is more accurate with respect to the real voltage measurement, however, it represents a higher computational cost, therefore the mean is calculated and improved by discarding data values in a transitory state, achieving better accuracy than the median to determine the real voltage value, enhancing the quality of the reconstructed images. A performance comparison between a personal computer (PC) and RPi4 is presented. The proposed EIT system offers an excellent cost-benefit ratio with respect to a traditional PC, taking into account precision, accuracy, energy consumption, price, light weight, size, portability and reliability. The proposed EIT system has potential application in mechanical ventilation, food industry and structural health monitoring. .

Keywords: Electrical impedance tomography; EIT; image reconstruction; single board computer; Raspberry Pi 4; electronic instrumentation.

Dedicatoria y agradecimientos

Dedicado a todas las personas que hicieron posible mi formación academica hasta el máximo grado existente en nuestro sistema, a mi esposa, mi familia, amigos, profesores, hasta los contribuyentes de quienes con sus impuestos se generan las becas de estudio.

Agradezco al Dr. Everardo Inzunza Gonzalez, al Dr. Oscar Roberto López Bonilla, director y co-director de tesis respectivamente, asímismo a los sinodales, el Dr. Enrique Efrén García Guerrero, la Dra. Almendra Villela y Mendoza, y al Dr. Jesús Everardo Olguín Tiznado, por su apoyo, guía y revisión durante los estudios y el trabajo de tesis de doctorado.

Agradezco al Consejo Nacional de Ciencia y Tecnología por la beca otorgada para poder realizar estos estudios.

Agradezco a la Universidad Autónoma de Baja California por la exención de pago de inscripción en alumnos becados

Esperando que en el futuro más personas tengan la oportunidad de estudiar y lograr terminar una carrera profesional, agradezco a todos quienes respetan la educación, ya que la educación, es la solución a la mayoría de nuestros problemas como sociedad y humanidad.

Table of Contents

Abstract III

Introduction 1

Background 3

Problem statement 5

Proposed solution 6

Research objectives 6

Specific research objectives 6

1. Basic principles of tomography 8
1.1. Tomography . . . 8
1.2. Tomography types and application areas . . . 9
1.3. Projection . . . 10
1.4. Image reconstruction . . . 11
1.5. Back-projection . . . 13
1.6. Mathematical expressions . . . 15
1.6.1. Projection . . . 15
1.6.2. Back-projection . . . 16
1.6.3. The Dirac function . . . 17
1.7. Overview . . . 19

2. Electrical Impedance tomography 20
2.1. Advantages and disadvantages of Electrical impedance tomography . . . 21
2.2. Mathematical approach . . . 21
2.2.1. Well posed and Ill posed problem definition . . . 22
2.2.2. Mathematical model . . . 22
2.3. Function diagram of an EIT system . . . 23
2.4. Methods of simulations and measurements for EIT . . . 24
2.4.1. Adjacent drive method . . . 25
2.4.2. Opposite method . . . 26
2.4.3. Cross method . . . 27
2.4.4. Trigonometric method . . . 28
2.5. Variations in Electrical Impedance Tomography . . . 29
2.6. Applications of Electrical Impedance Tomography . . . 29
2.6.1. Lung . . . 29
2.6.2. Breast and Cervix . . . 29
2.6.3. Brain . . . 30
2.6.4. Overview . . . 30
2.7. EIDORS library . . . 30

3. System development **31**
3.1. Adjacent measurement method . . . 31
3.2. Test unit (vessel) . . . 32
3.3. Electronic design . . . 33
3.3.1. Constant current source . . . 34
3.3.2. CMOS multiplexer . . . 36
3.3.3. High-precision peak detector . . . 36
3.3.4. Analog-to-digital converter (ADC) . . . 38
3.4. Firmware and functions for the proposed EIT system . . . 39
3.4.1. Data acquisition firmware . . . 39
3.4.2. Firmware for data comparison . . . 40
3.4.3. Function for statistical analysis . . . 42
3.4.4. Firmware for calibration and real-time working . . . 43
3.4.5. Image reconstruction . . . 44

4. Experimental results **47**
4.1. Comparison between the PC and RPi4 . . . 47
4.1.1. Calibration of the proposed EIT system . . . 47
4.2. Orange as test unit . . . 48
4.3. Real-time results on RPi4 . . . 49
4.4. Performance comparison between PC and RPi4 . . . 52
4.5. Comparison versus related work . . . 54
4.6. Pictures of the EIT device working on PC using Matlab and on RPI4 Using GNU Octave . . . 56

5. Conclusions **58**
5.1. Future Work . . . 59

6. Printed Circuit Boar design **61**

List of Figures

1. Vessel with object of study Ω. There are 16 electrodes around the vessel, I represents the current injected, and V_1 the voltage measurements and Ω represents the sample core, taken from Molinari (2003). . . . 2
2. Basic tomography, the emitter sends a signal, this signal passes through the object and changes because of its natural characteristics, creating a projection, then a receiver captures this signal to gather data that will be process to make an image reconstruction. . . . 8
3. Simple tomography projection. Taken from (Zeng, 2009). . . . 10
4. Projections are different, they are angle dependent. Taken from (Zeng, 2009). 11
5. A sinogram is a representation of the different projections on the plane $s - \theta$. Taken from (Zeng, 2009). . . . 11
6. Point source object projection. . . . 12
7. Image reconstruction of a point source by non filtered and filtered back-projection. Taken from (Zeng, 2009). . . . 13
8. View to view projection. Taken from (Zeng, 2009). . . . 14

9. Sum of all back-projections. Taken from (Zeng, 2009). 14
10. Coordinate system for parallel beam 2D imaging. Taken from (Zeng, 2009). . 15
11. Entrances a_{ij} of Matrix A 16
12. Vessel with object of study Ω, there are 16 electrodes around the vessel, I represents the current injected, and V_1 the voltage measurements, Ω represents the sample core. taken from (Molinari, 2003). 23
13. General diagram of an EIT system. 24
14. Adjacent measurement or neighboring method, a) First set of measurements while injecting current between electrode 1 and 2, b) Second set of measurements while injecting current between electrode 2 and 3, taken from (Harikumar et al., 2013). 26
15. Opposite or polar drive pattern method, a)First set of measurements while injecting current between electrodes 1 and 9 (180° apart), b)Second set of measurements while injecting current between electrodes 2 and 10 (180° apart), taken from (Harikumar et al., 2013). 27
16. Cross or diagonal drive pattern method, a)First set of measurements while injecting current between electrodes 16 and 2, b)Second set of measurements while injecting current between electrodes 16 and 4, taken from (Harikumar et al., 2013). 28
17. Electrical Impedance Tomography (EIT) of thoracic cavity to lung function, taken from (Rai et al., 2013). 29
18. Test unit (vessel) with 16 stainless steel of 304-caliber electrodes. 31
19. Adjacent measurement method, taken from Calvo Hernando (2018). (a) First measurement process, the current is injected between electrodes 1 and 2, (b) Second measurement process, the current is injected between electrodes 2 and 3. 32
20. Test unit with 16 electrodes, counterclockwise enumerated. 33
21. Block diagram of the proposed EIT system. (a) Data acquisition stage, (b) User interface. 34
22. Constant current source circuit is 91,42 μA. 35
23. Output current sensitivity to load impedance changes: (a) from 0 to 120 kΩ the current remains fixed at 91,42 μA, a higher impedance value falls out of the fixed current range; (b) the voltage in CSp_1 yields to voltage saturation of the TL084 op-amp when the load is higher than 120 kΩ. 36
24. Proposed high-precision peak detector. 38
25. Peak signal detected by the high-precision peak detector. 38
26. Three graphs of a measurement cycle. (a) Comparison between calibration data and arbitrary object data, (b) Calibration data and second round of calibration-plane measurements, and (c) Percentage of error between calibration data and the second round of measurements. 41
27. Four graphics showing measurements for four different electrode pairs, taken with the proposed EIT system by acquiring 250 samples. A transient voltage behavior is observed. (a) First pair of electrodes, (b) Second pair of electrodes, (c) Third pair of electrodes, and (d) Fourth pair of electrodes. 43
28. Test unit (vessel) with only conductive water to perform calibration. 48

29. Comparison of measurements for image reconstruction between the PC and RPi4. (a) Measurements corresponding to the calibration plane using the PC, (b) Measurements corresponding to the calibration plane using RPi4, (c) Second round of calibration-plane measurements using the PC, (d) Second round of calibration plane measurements using RPi4, (e) Differences between first and second-round measurements using the PC, (f) Differences between first and second-round measurements using RPi4. 48
30. Comparison of image reconstruction for the calibration plane on the PC versus RPi4: (a) Image reconstruction using a 4 kHz signal, with no object inside the vessel and data processing on the PC, (b) Image reconstruction using a 4 kHz signal, with no object inside the vessel and data processing on RPi4. 49
31. Test of the proposed EIT system using an orange as the test unit. (a) Orange in the calibration plane, (b) Image reconstruction of orange in the calibration plane, (c) Orange with seawater injected, (d) Image reconstruction of orange with seawater injected. 50
32. Real-time image reconstruction on RPi4: (a) Glass object under test, (b) Metal object under test, (c) Metal and glass object under test, (d) Metal and glass in different positions, (e) Metal and glass in different positions, (f) An orange under test. 51
33. Picture of the proposed EIT system using a PC. 56
34. Picture of the proposed EIT system using RPi4. 57
35. Circuit designed for the proposed EIT system. 61
36. PCB designed for the proposed EIT system. 62
37. Gerber designed for the proposed EIT system. 62
38. Printed circuit board with components of EIT system. 63

List of Tables

1. Proposed EIT system features. 34
2. Measurements for output current sensitivity to load impedance changes test. 37
3. Comparison of characteristics of the proposed EIT on the PC versus RPi4. . 53
4. Comparison between the execution times of the algorithms on a PC vs. RPi4 54
5. Comparison of proposed EIT system versus other related work. 55

Introduction

Electrical impedance tomography (EIT) is a non-invasive technique that consists in measuring an impedance array through a cross-section. This technology has been applied in many clinical applications Sapuan et al. (2020); Dunne et al. (2018); Samorè, A. and Guermandi, M. and Placati, S. and Guerrieri, R. (2017), such as detection for breast cancer Hu and Soleimani (2020); Pak et al. (2012), nerve activity in the brain Makarov et al. (2019); Faulkner et al. (2018); Aristovich et al. (2016), respiratory disorders Seward et al. (2019); Gow et al. (2018); Karsten et al. (2013), lung function detection Ain et al. (2017); Huang et al. (2016); Frerichs et al. (2002), cardiovascular monitoring Rapin et al. (2019), assess facial nerve proximity Anso et al. (2019), also has several industrial applications Wang et al. (2019); Liu et al. (2019); Ryndin et al. (2018); Dupré and Mylvaganam (2018); Wu et al. (2018); Russo et al. (2017a); Silvera-Tawil et al. (2015), and structural health monitoring in the construction industry Saibaba et al. (2014); Zhang et al. (2009); Aydi et al. (2020); Wei and Gao (2017); Gao et al. (2019); Badr et al. (2019); Priou et al. (2019). The food industry also uses electrical or electrochemical impedance spectroscopy (EIS) which in simple terms is a kind of EIT by using multiple frequencies and it is used in food quality assurance to detect adulterated or polluted food, the electrical parameters of food change when they are adulterated, as well when food has a pathogen like bacteria Das et al. (2018); Mane and Mudhalwadkar (2017); Ibba et al. (2018); Serena Chiriaco et al. (2018). The impedance of human body tissue is able to provide information about the physiological and pathological properties of the tissue, both of these properties are related to the information of medical applications Sapuan et al. (2020). EIT can be achieved by using multiple electrodes placed in a cross-section, however this is not mandatory and other configurations of EIT can be used. Electrodes are important components of EIT system, they must have good electrical conductivity and must be anti-corrosive because an electrical current is applied through them and also are used for sensing voltage. There is a research work focused on the study of electrodes, because they can be improved for example through sandblasting Gatabi et al. (2020). The data obtained by measuring all possible impedances is used to reconstruct an image, which may provide qualitative and quantitative information. Images of live tissues and organs can be obtained by placing electrodes on the skin and injecting a small current into the body. EIT could provide a safe and cost-effective alternative to established clinical imaging met-

hods across a wide range of applications. However, the imaging problem is severely ill-posed (inverse problem) and ill-conditioned, which means that even relatively low noise levels in measurements could lead to significant reconstruction artifacts. In other words, the solution is highly sensitive to changes in the final data Dimas et al. (2020); C. Dimas, N. Uzunoglu, P. P. Sotiriadis (2019) and therefore the resulting image quality is limited Malone et al. (2015); Russo et al. (2017b).

Figure 1 shows a basic 16-electrode system. The main equation for the voltage field produced by running a current across a material corresponds to (1), where I is the current, σ is the electric impedance of the medium, ϕ is the electric potential, ω is the angular frequency, and ϵ is the electric permittivity. This equation can be reduced to an equation known as the "standard governing equation for EIT" Stacey (1986), given in (2),

$$\nabla \cdot (\sigma + I\omega\epsilon)\nabla\phi = 0, \tag{1}$$

$$\nabla \cdot (\sigma\nabla\phi) = 0. \tag{2}$$

The problem requires the injected current I and the voltage measured V_1, the values of which are known and obtained from an EIT electronic system, but the impedance distribution σ is unknown; here we cannot easily resolve σ for (2) because the potential distribution ϕ is a function of the impedance, $\phi = \phi(\sigma)$. As mentioned before, here the ill-posed nature of the problem is clear from observing and understanding the diffusive behavior of electricity and the inherent measurement errors.

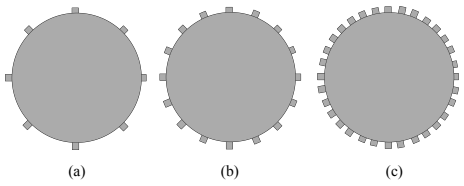

Figure 1: Vessel with object of study Ω. There are 16 electrodes around the vessel, I represents the current injected, and V_1 the voltage measurements and Ω represents the sample core, taken from Molinari (2003).

As a tomography technique, EIT basically reconstructs the spatial distribution of electrical conductivity within a body by measuring the voltage that appears on object boundaries due to the flowing electrical current Cagan and Rosler (2017). The basic principle is to use the material's impedance features to characterize its internal structure Mao et al. (2019). Some

authors argue that it is an emerging method for imaging the evoked activity of a rat brain Hannan et al. (2020); Faulkner et al. (2018), and it can also be used in human brain injury monitoring, as reported in Ma et al. (2019); Shi et al. (2018).

Backgroung

As mentioned above, EIT has been studied since the 1980s, research in this area comprehend different works, some of this are detailed below. The authors in Avery et al. (2017) developed a highly versatile ElT system using open-source software and commercial components. The system design was shared under an open-source license and uses electronic modules and a personal computer (PC) interface. Their results can be confirmed by comparing the reconstructed images with well-known literature. Field-programmable gate array (FPGA) devices have been used to develop EIT, as shown in Sohal et al. (2014); Kusche et al. (2015), basically to control and execute commands for the EIT system, leveraging the advantages they offer as programmable gates. Their complexity enabled the authors to deliver high-speed and high-performance results. Other efforts are being made for EIT algorithms based on back-projection, Fourier, Gauss-Newton and variable splitting (VS) Wang et al. (2019). Other authors have worked on developing an approach to EIT image reconstruction based on machine-learning algorithms, proving that neural networks are useful for EIT Fernández-Fuentes et al. (2018). In Liu et al. (2018), the authors propose an efficient and high-resolution EIT image reconstruction method in the framework of sparse Bayesian learning. Significant performance improvement is achieved by imposing structure-aware priors on the learning process to incorporate the prior knowledge that practical conductivity distribution maps exhibit clustered sparsity and intra-cluster continuity. In Liu et al. (2021), the authors propose an efficient and high-spatial-resolution algorithm for simultaneously reconstructing multiple fdEIT (Frequency-difference electrical impedance tomography) frames corresponding to inject currents with multiple frequencies. The electrical impedance tomography reconstruction problem is considered within a hierarchical Bayesian framework, where both intratask spatial clustering and intertask dependency are automatically learned and exploited in an unsupervised manner.

Other research efforts have focused on designing nine different circuits for EIT systems

and comparing three different solutions using a digital signal processor (DSP) for image reconstruction, resulting in a low-cost system Santos and Simini (2012). The use of eight silver electrodes distributed in a ring configuration to make electrical impedance measurements is reported in Gutierrez-Lopez et al. (2019) as a methodology for locating carcinoma, together with a proposed algorithm that is used in breast models. A study employing active electrodes for lung ventilation is reported in Gaggero et al. (2012), which presented an electronic system and experimental results on a human being, proving that active electrodes can be applied for human thoracic EIT. The system communicates through Ethernet to a PC or ventilator and uses an FPGA to control impedance sampling. As can be inferred, one of the many problems with working with humans is placing electrodes in a person, and in addition, electronic noise can be generated by skin, hair or sweat. With some reservations, the authors achieved good results for future medical applications of EIT.

From a hardware viewpoint, the authors in Deng et al. (2018) developed a parallel EIT system using multiple microcontroller units (MCUs) to perform measurements and process FFTs at the same time. The system, which reaches speeds of up to 30 frames per second, was compared to a commercial one, and an error rate of only 10 % was found. The authors in Ansory et al. (2018) report the development of an EIT system with an Arduino MCU and the well-known Electrical Impedance and Diffuse Optical Tomography Reconstruction Software (EIDORS) Adler and Lionheart (2006) on a PC, using Matlab to reconstruct images. The system has a resolution of 32 electrodes and each part of the system is developed on separate PCBs (Printed circuit boards). They reconstruct images, but in contrast with this Ph.D thesis, their ADC only has a resolution of 12 Bit, their circuits and algorithms are not described in detail, and they do not perform image reconstruction on a SBC. In Widodo Aris (2018), the authors report an EIT system developed using an Arduino MCU, a Raspberry Pi 3 and 16 electrodes. They shown that the system reconstructs images by using Python software instead of the EIDORS Adler and Lionheart (2006) library for Matlab. The authors in Borsoi et al. (2018) present a super-resolution imaging model for EIT, with results that show better image quality using different simulated data. On that basis, in this study the EIDORS library was used to perform image reconstruction. In addition, the authors in Sapuan et al. (2017) developed an EIT system that combines the reconstruction of three different images at different frequencies, with the goal of simulating a breast tumor and showing the

importance of obtaining images with different frequencies to obtain better information. More recently, the authors in Perchiazzi and Wrigge (2019) reviewed different studies of imaging techniques, including EIT, and reported that Acute Respiratory Distress Syndrome (ARDS) problems had only been partially resolved. The literature review leads us to assert that EIT can be employed in cases of respiratory conditions Gow et al. (2018); Perchiazzi and Wrigge (2019); Wu et al. (2018); Putensen et al. (2019); Zhang et al. (2019); Akhavan and Hashemian (2018); Wu et al. (2019). For this reason, further research and development in EIT lung imaging is crucial.

Accordingly, one can take advantage of SBC, which are very useful for solving real-world problems across various fields of application Alessio et al. (2020); Nykvist et al. (2020); Aguirre-Castro et al. (2019); Gautam et al. (2020); Nirmala and Malarvizhi (2020). To our knowledge and based on the reviewed literature, only one study reports the use of an Raspberry Pi 3 Model B Widodo Aris (2018), and one other paper reports using an Arduino MCU Ansory et al. (2018) for the development of an EIT system. However, there are still open problems to be solved, such as the development of new methods and algorithms to improve EIT systems, because of the imaging problem is severely ill-posed and ill-conditioned, which means that even relatively low noise levels in measurements could lead to significant reconstruction artifacts. Thus, in this Ph.D thesis an RPi4 may prove useful in developing a low-cost, portable and reliable EIT system, since it can be coded by using open-source software and is inexpensive, small, and lightweight; furthermore, it performs well and offers multiprocessing capabilities and easy scheduling tasks, thus enabling fast technological development. The novelty of this Ph.D thesis is the development of three simple and efficient algorithms that can be implemented on SBC. Details of the new electronic circuits, firmware and functions developed in this study are presented herein. The experiments show that the proposed EIT system delivers practically the same results as those obtained with a traditional PC.

Problem statement

Electrical impedance tomography (EIT) has 40 years of research, among its advantages it offers a low cost solution compared to another kind of tomography techniques, as the com-

puter axial tomography, or Magnetic Resonance tomography, which have complex medical applications, but are not necessarily needed all the time, EIT for lung imaging has been useful for medical pulmonologist. There are research about development of electrical systems for EIT which are complemented with software developed in personal computers. This means that nowadays EIT tomographers are implemented with personal computers, that require space, energy consumption and not much portability.

- Actual methods realized filtering with analogical electronics, which implied phisical circuits, and energy consumption.

- Algorithms of EIDORS library require data obtained from a high precision stage.

Proposed solution

In this research, a new electrical impedance tomography system is proposed, by using high precision electronic components, an embedded stage of data acquisition by using ATMEGA2560 microcontroller, and a dual option of using SBC Raspberry Pi 4 or Personal computer, which receive data and process it in Octave GNU with EIDORS library to perform image reconstruction, SBC Raspberry Pi 4 proves reliability and has multiples cost-benefit advantages in comparison with a PC.

Research objectives

The main research objective is the development of a system for image reconstruction from electrical impedance tomography using free software and a single board computer.

Specific Research objectives

- Design and develop the necessary circuitry for signal conditioning related to obtain data from impedance measurements.

- Develop of pre-processing techniques for data smoothing using known statistical tools.

- Develop algorithms for data acquisition, calibration, comparison and real time operation.

- Image reconstruction using EIDORS library from electrical impedance tomography measurements.

- Perform an analysis of system reliability and performance.

Chapter I

1. Basic principles of tomography

The following concepts in this chapter were studied and are in part, a summary of basic principles of tomography taken from (Zeng, 2009).

1.1. Tomography

Tomography is a word coming from ancient greek word "tomos" which means "slide or section" and "grafo" which means "to describe or to write", tomography is also known as imaging, a device that performs tomography or imaging is called a tomograph, and its resulting image is called a tomogram. In order to create a tomogram, there should be an image reconstruction process, this theory was first proposed by Johann Radon in 1917 (Radon, 1917). A tomographic system consists in the use of transducers at certain frequencies, which send signals and receive other reflected of modified signals that contain information. A basic diagram is shown in Figure 2. In medicine, tomography is widely used because its advantage of obtaining information without the need of open a body, therefore tomography uses non destructive techniques.

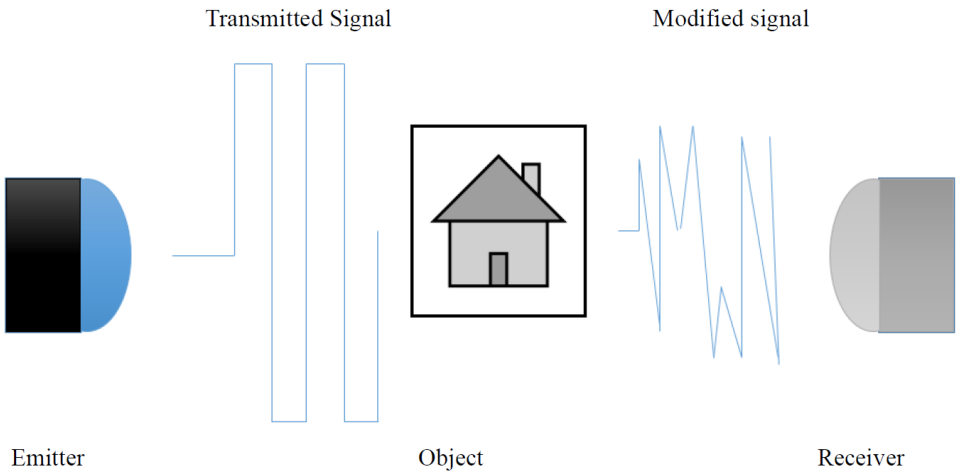

Figure 2: Basic tomography, the emitter sends a signal, this signal passes through the object and changes because of its natural characteristics, creating a projection, then a receiver captures this signal to gather data that will be process to make an image reconstruction.

1.2. Tomography types and application areas

Tomography types are normally divided according to the frequency and method that uses, nowadays the next types of tomography exists:

- Electrical impedance tomography: Its principle is to measure the internal set of impedance of an object when electrical current signals are applied.

- Ultrasonic tomography:Is the kind of tomography where ultrasound is used, that is to say signals above the 20 kHz to 20 MHz, though that depends in the resolution and data type that is willing to be obtained, in the ultrasound tomography echo measurements can be applied, to make measurements and also it may consider the Doppler effect, which measures the frequency variation of the signal, this last is used for fluids and is widely used in medicine.

- Magnetic resonance tomography: Most known as magnetic resonance imaging (MRI), is based in the nuclear magnetic resonance principle, to obtain data from a studied object, it uses magnetic fields, therefore is not invasive, and is very used in medicine.

- Computed axial tomography: Best known as CT, is uses the image reconstruction principle of Johann Radon, the signals applied by this technique are X rays, which means that is invasive and it is widely used in medicine.

There are more tomography types, which most of its application and field are for medical purposes, however, there are industrial applications in other fields as in geology, tomography can be applied to:

- Patology detection in the medical field, intern organ explorations, tomography is most used in medicine.

- Preliminary studies for the design of civil works to determine the depth to the basement.

-Applications in geology such as determination of stratigraphy and detection of cavities, water table and saline intrusion.

- Tridimentional structure obtaining (scanning an area and receive a 3D model of the area scanned).

- Tree growth studies.

1.3. Projection

A projection, is an image generated in the study of an object, in Figure 3, it is observed in first instance, a disc with center at the origin and lineal density ρ, the projection of this object can be calculated as the curve length t times the lineal density ρ.

In this example the projection $p(s)$ is the same for every angle view θ, which is the detector orientation, when the object is more complex, then the projection becomes dependent of the θ angle, then now we have $\rho(s, \theta)$.

$$p(s) = \begin{cases} \rho t = 2\rho\sqrt{R^2 - s^2}, & |s| < R, \\ 0, & |s| \geqslant R. \end{cases}$$

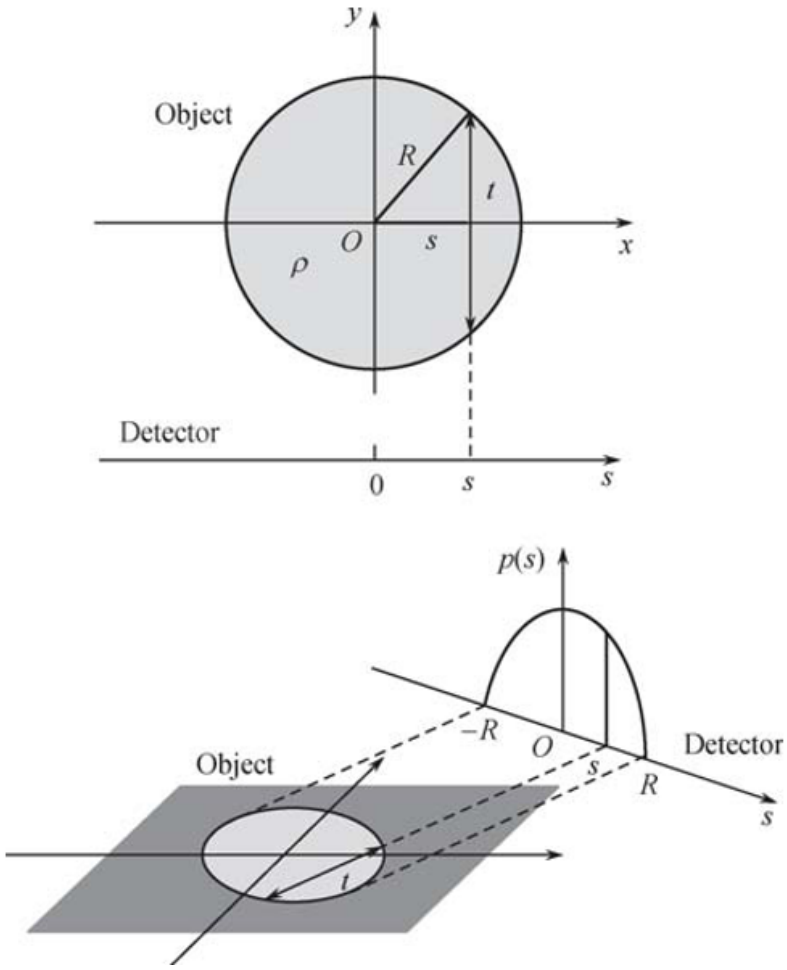

Figure 3: Simple tomography projection. Taken from (Zeng, 2009).

When depending also of the angle, different projections are generated as we variate θ,

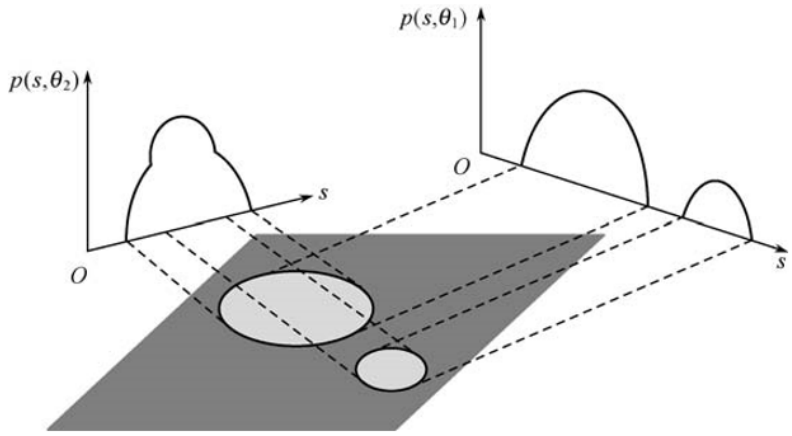

Figure 4: Projections are different, they are angle dependent. Taken from (Zeng, 2009).

The next example uses a source point in the y axis to illustrate the θ angle dependency of the $\rho(s,\theta)$ projection Figure 5).

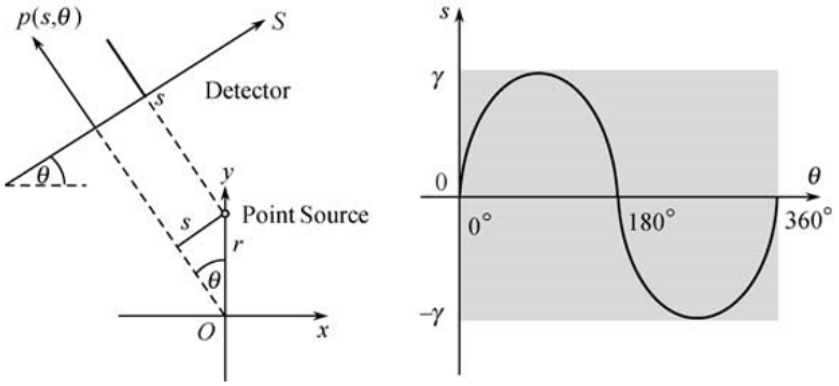

Figure 5: A sinogram is a representation of the different projections on the plane $s-\theta$. Taken from (Zeng, 2009).

1.4. Image reconstruction

A strategy to perform an image reconstruction considering a point source is this: Let's consider a two dimentional empty plane, with a coordinate system x, y, and colocate a small point with a value of 1, somewhere on that plane and not necessarily in the origin (Figure 6). Now let's imagine that there is a detector, a camera for example, making turns around the origin, acquiring projection images. In a particular angle θ, let's write the projection as $\rho(s,\theta)$, where s is the coordinate on the detector.

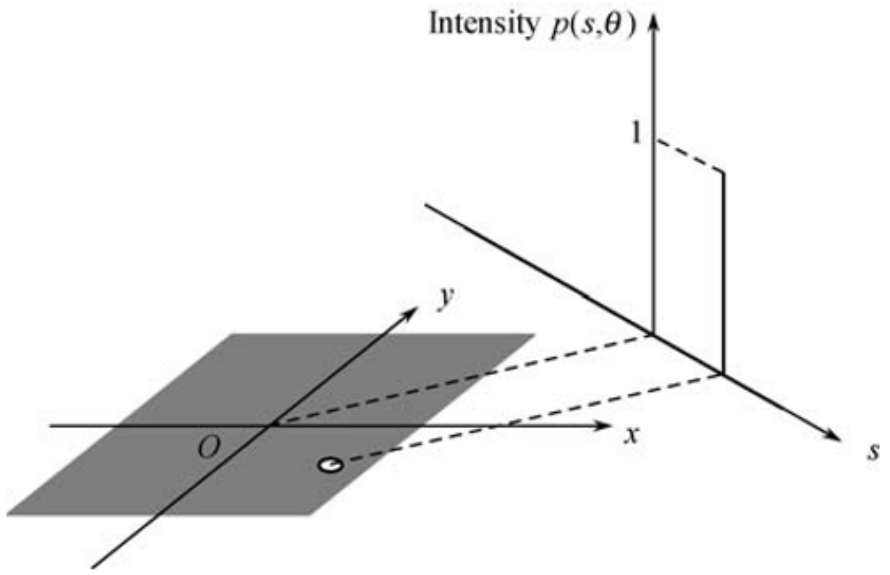

Figure 6: Point source object projection.

The $\rho(s, \theta)$ projection is formed drawing a line through the x, y plane, orthogonal to the detection, and finding on the detector in the place s. Then, a line integral is evaluated along this line, and the integral value is $\rho(s, \theta)$, in this example, if the line does not touch the point source, then $\rho(s, \theta)$ is zero, if the line passes through the point source $\rho(s, \theta)$ then is 1.

Now let's proceed to make an image reconstruction using the $\rho(s, \theta)$ projections. As shown in Figure 7, a number of projections are taken from the point source at different visual angles. Now let's proceed to reconstruct the punctual source as follows.

When we see the $\rho(s, \theta)$ projections from a θ angles, it can be appreciated a pike with intensity of 1. This pike is the sum of all activity along the projection path. To reconstruct the image, the activity must be redistribute in the return pike to its original path. The problem lies in it is not known where should more activity must be placed along the path, and where to put less. Therefore, equal amounts of activity are placed in all places along the path, and the quantity is the magnitude of the projection pike. If this process is continually made for more angles, a high pike will be form in the x, y plane in the location of the point source, due to the superposition effect.

The above is a standard procedure called back-projection, if we back-project from all angles from 0° to 360° it will produce a signal as shown in the image. After back-project, the image is not exactly the original, but a blurred version, to eliminate this effect, negative wings

are introduced around the pike in the projections before back-projecting, this process is called filtration. The use of negative wings gives us a clean image. This image reconstruction algorithm is common and it is referenced as the filtered back-projection algorithm (FBP).

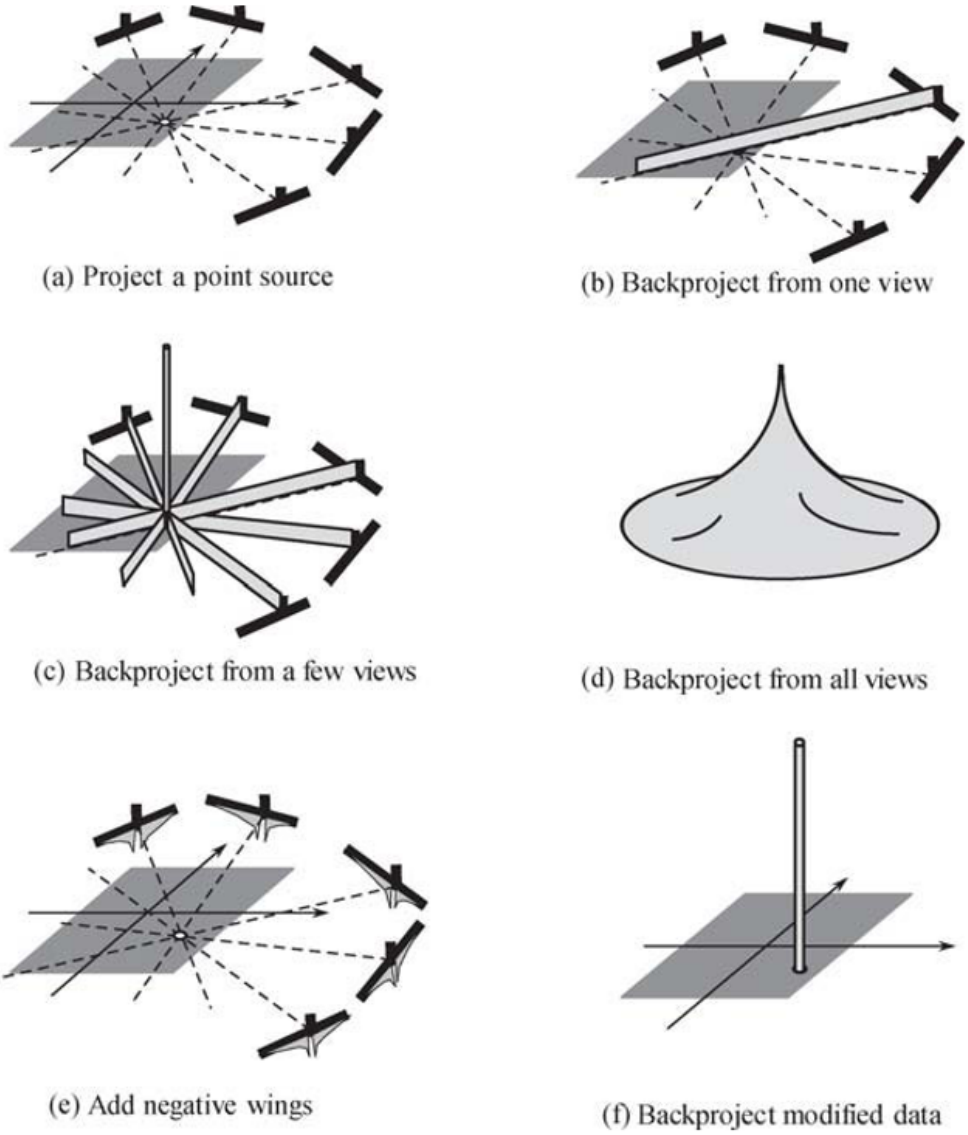

Figure 7: Image reconstruction of a point source by non filtered and filtered back-projection. Taken from (Zeng, 2009).

1.5. Back-projection

Back-projection is not the inverse of a projection, a back-projection is not enough to perform an image reconstruction, after back-projecting data, the original image is not obtained. This is explained by a simple problem of 2×2:

The original image is defined by $x_1 = 3, x_2 = 2, x_3 = 4$ y $x_4 = 0$. The associated projections are $\rho(1, 0°) = 7, \rho(2, 0°) = 2, \rho(1, 270°) = 5$ and $\rho(2, 270°) = 4$. The projections are formed from a view at certain time.

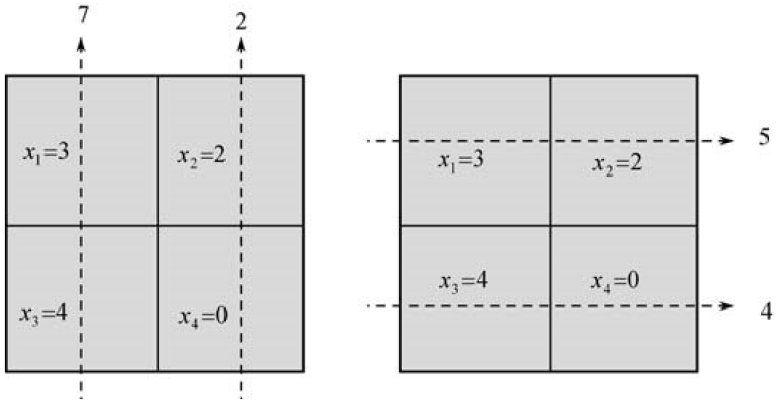

Figure 8: View to view projection. Taken from (Zeng, 2009).

The back-projected image is formed wiew to viwe. The final back-projected image is the sum of the back-projections from all views, as shown in Figure 9. Notice that the back-projected image is different than the original.

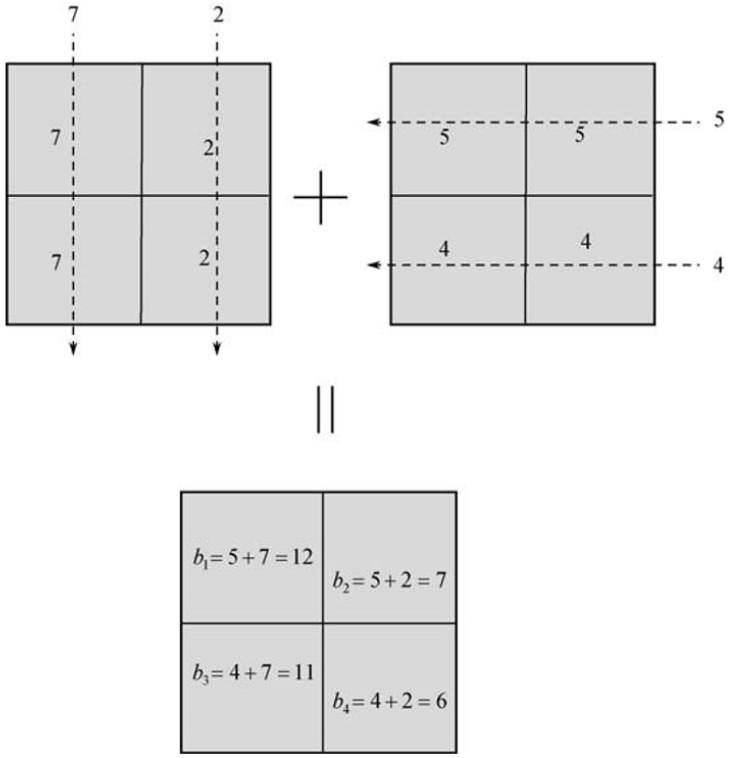

Figure 9: Sum of all back-projections. Taken from (Zeng, 2009).

1.6. Mathematical expressions

1.6.1. Projection

Let $f(x, y)$ be a function density in the $x-y$ plane. The projection (ray, sum, line integral or Radon transform) $p(s, \theta)$ has many equivalent expressions as follows:

$$p(s,\theta) = \int_{-\infty}^{\infty}\int_{-\infty}^{\infty} f(x,y)\delta(xcos\theta + ycos\theta - s)dxdy \tag{3}$$

$$p(s,\theta) = \int_{-\infty}^{\infty}\int_{-\infty}^{\infty} f(x,y)\delta(x\theta - s)dxdy \tag{4}$$

$$p(s,\theta) = \int_{-\infty}^{\infty} f(s\theta + t\theta\ \perp)dt \tag{5}$$

$$p(s,\theta) = \int_{-\infty}^{\infty} f_\theta(s,t)dt \tag{6}$$

Where δ is the Dirac delta function, and f_θ if the f function rotated by θ clockwise. It is assumed that the detector rotates in this sense around the object, or that the object rotates in this sense while the detector is still. The coordinate system is shown in Figure 10.

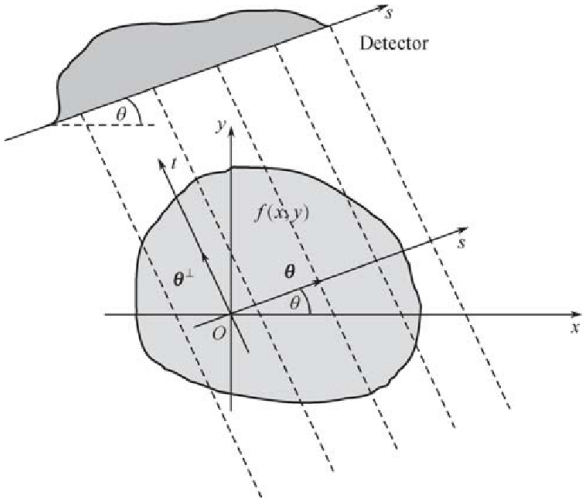

Figure 10: Coordinate system for parallel beam 2D imaging. Taken from (Zeng, 2009).

1.6.2. Back-projection

A back-projection is the assistant of a projection. Assistant means a mathematical term. It means the transposed conjugate in linear algebra. For a real matrix A its assistant is simply the transposed of the A^T matrix. In the discreet case, the projection is:

$$P = AX \tag{7}$$

Where X represents an image, but in column form. Taking the matrix from Figure 8, the image 2×2 is expressed by:

$$X = [x_1, x_2, x_3, x_4]^T \tag{8}$$

The column matrix P represents the projections.

$$P = [p(1, 0°), p(2, 0°), p(1, 270°), p(2, 270°)]^T = [7, 2, 5, 4]^T \tag{9}$$

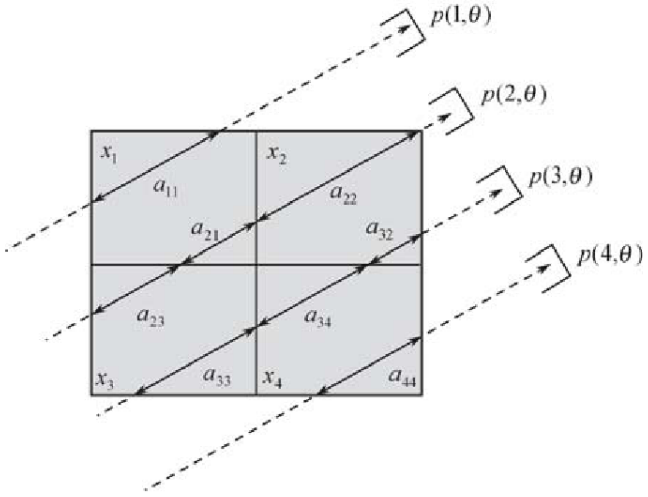

Figure 11: Entrances a_{ij} of Matrix A

Matrix A is the projection operator. Its entrances a_{ij} are defined in Figure 11, using the example of Figure 8, the back-projection of P can be calculated using the following matrix multiplications:

$$B = A^T P = \begin{bmatrix} 1 & 0 & 1 & 0 \\ 0 & 1 & 0 & 1 \\ 1 & 1 & 0 & 0 \\ 0 & 0 & 1 & 1 \end{bmatrix} \begin{bmatrix} 7 \\ 2 \\ 5 \\ 4 \end{bmatrix} = \begin{bmatrix} 1 & 0 & 1 & 0 \\ 0 & 1 & 1 & 0 \\ 1 & 0 & 0 & 1 \\ 0 & 1 & 0 & 1 \end{bmatrix} \begin{bmatrix} 7 \\ 2 \\ 5 \\ 4 \end{bmatrix} = \begin{bmatrix} 12 \\ 7 \\ 11 \\ 6 \end{bmatrix}$$

(10)

Which is the same graphically obtained result in Figure 9. For the continuous case, the back-projected image $b(x, y)$ can be expressed in the next equivalent way:

$$b(x, y) = \int_0^{\pi} p(s, \theta)|_{s=xcos\theta+ysin\theta} d\theta \tag{11}$$

$$b(x, y) = \frac{1}{2} \int_0^{2\pi} p(xcos\theta + ysin\theta, \theta) d\theta \tag{12}$$

1.6.3. The Dirac function

The Dirac function δ is a generalized function or a distribution function. It can be defined in different ways. In this case, Gaussian functions series are used to define the δ function. Each one of the Gaussian functions have an area unit below its curve, and as n increases, the curve becomes more high and narrow.

$$(\frac{n}{\pi})^{1/2} e^{-nx^2} \tag{13}$$

Let's consider $f(x)$ a smooth function which is differentiable in any place and any order and $\lim_{x\to\infty}(x^N)f(x) = 0$ for every N. Thus the function δ is implicitly defined as:

$$\lim_{x\to\infty} \int_{-\infty}^{\infty} (\frac{n}{\pi})^{1/2} e^{-nx^2} f(x) dx = \int_{-\infty}^{\infty} \delta(x) f(x) dx = f(0) \tag{14}$$

δ function has some properties:

$$\int_{-\infty}^{\infty} \delta(x - a) f(x) dx = \int_{-\infty}^{\infty} \delta(x) f(x + a) dx = f(a) \tag{15}$$

$$\int_{-\infty}^{\infty} \delta(ax)f(x)dx = \frac{1}{|a|}f(0) \tag{16}$$

$$\int_{-\infty}^{\infty} \delta^{(n)}(x)f(x)d(x) = (-1)^n f^{(n)}(0) \tag{17}$$

n-nth derivative order

$$\delta(g(x))f(x) = \sum_n \frac{1}{|g'(\lambda_n)|}\delta(x-\lambda_n) \tag{18}$$

Where λ_n's are the zeros of $g(x)$. In 2D and 3D cases, $\delta(x) = \delta(x)\delta(y)$ and $\delta(x) = \delta(x)\delta(y)\delta(z)$, respectively. In the last property, $|g'|$ will be replaced by $|grad(g)| = \sqrt{(\frac{\partial g}{\partial x})^2 + (\frac{\partial g}{\partial y})^2}$ and $|grad(g)| = \sqrt{(\frac{\partial g}{\partial x})^2 + (\frac{\partial g}{\partial y})^2 + (\frac{\partial g}{\partial z})^2}$, respectively in 2D and 3D. In 2D imaging. A δ $\delta(x-x_0)$ function is used to represent a point source in the $x = x_0$ location. The Radon transform of $f(x) = \delta(x-x_0)\delta(y-y_0)$ is:

$$p(s,\theta) = \int_{-\infty}^{\infty}\int_{-\infty}^{\infty} \delta(x-x_0)\delta(y-y0)\delta(xcos\theta + ysin\theta - s)dxdy \tag{19}$$

$$p(s,\theta) = \int_{-\infty}^{\infty} \delta(y-y0)[\int_{-\infty}^{\infty} \delta(x-x_0)\delta(xcos\theta + ysin\theta - s)dx]dy \tag{20}$$

$$p(s,\theta) = \int_{-\infty}^{\infty} \delta(y-y0)\delta(x_0cos\theta + ysin\theta - s)dy \tag{21}$$

$$p(s,\theta) = \delta(x_0cos\theta + y_0sin\theta - s) \tag{22}$$

This is a sinogram.

1.7. Overview

In general terms, the basic principles of tomography are given by mathematical expressions that were defined in 1917 by Johann Radon, this mathematical definitions helped to develop tomography systems as we know today, the first devices that were invented had many issues as for example the required time to perform a tomography, the first X-ray tomographers took about 20 minutes to perform a scan, which is a lot time for a person to be exposed to this ionized energy, overtime, systems became more efficient and effective, but all the original theory remains the same for most of the modern tomography.

Chapter II

2. Electrical Impedance tomography

Electrical properties as the electrical conductivity σ and the electric permittivity ϵ, determine the behaviour of materials under the influence of external electric fields. This means that conductive materials have a high conductivity which allows direct and alternating currents to flow, whereas dielectric materials have a large electric permittivity and only allow passage of alternating current. Electrical impedance tomography (EIT), has a different approach to conventional tomography, this mainly because its mathematical principle, EIT is a non-invasive technique which consists in measuring an impedance array through a cross-section. The way for obtaining data consists in measuring impedances through electrodes that are placed in an object, mostly in circular form, this impedances area measured not only in one way, but many paths, the more impedances are measured, the best image reconstruction can be made. EIT basically reconstructs the electrical conductivity spatial distribution within a body by measuring a voltage on objects boundaries that appear due to the flowing electrical current (Cagan and Rosler, 2017), its basic principle is to use the material's impedance features to perform the characterization of its internal structure (Mao et al., 2019).

Electrical impedance tomography features: - It is a tomography method that uses electrical current at low frequencies and low current.

- It is a method that is sensitive to electrical conductivity changes.

- Known current values must be applied, voltages are measured and by ohm's law, impedances are calculated.

- As frequency increases this method may show changes in the dielectric constant (also known as relative permittivity).

- It is useful in industry, geophysics, and has medical applications that are in development.

2.1. Advantages and disadvantages of Electrical impedance tomography

The main advantages of EIT are (Bera, 2018):

- Low cost prices in hardware.

- Non invasive.

- More portable than other types of tomography.

- Useful in applications where impedance value changes means useful data.

- Has scientific open access developed tools (EIDORS library).

The main disadvantages or EIT are (Bera, 2018) :

- Has poor Signal-to-Noise Ratio (SNR).

- Has poor spatial resolution.

- Although increasing number of electrodes increases spatial resolution is not always possible in real applications.

- EIT values of current injected have to be careful chosen for biological applications.

- Because of its nature as ill-posed inverse problem, EIT produces a large noise at the output in response to the small error or noise at the input.

2.2. Mathematical approach

Mathematically is a non-linear and ill posed problem, it is known as inverse Calderon problem (Caro et al., 2013), which objetive is to recover the coefficient of divergence in a differential partial elliptic equation given its Dirichlet to Neumann or Neumann to Dirichlet operator.

2.2.1. Well posed and Ill posed problem definition

According to Hadamard a well posed problem should be a Cauchy problem of initial value that has adequate analytic properties, whose possible solutions have a convenient structure, in particular this includes:

i) The existence of a solution.

ii) The solution uniqueness.

iii) The solution depends in a continuous way of the initial conditions

An ill posed problem does not meets one of the above situations, most of inverse problems are ill posed problems.

2.2.2. Mathematical model

Figure 12 shows a basic 16 electrode EIT system, the main equation for the voltage field produced by placing a current across a material corresponds to equation 23, where σ is the electric impedance of the medium, ϕ is the electric potential, ω is the frequency and ϵ is the electric permittivity. This equation can be reduced to a equation known as "standard governing equation for EIT" shown in equation 24

$$\nabla \cdot (\sigma + l\omega\epsilon)\nabla\phi = 0 \tag{23}$$

$$\nabla \cdot (\sigma\nabla\phi) = 0 \tag{24}$$

The problem requires the injected current i and the voltage measured v which values are known and obtained from an EIT electronic system, but the impedance distribution σ is unknown, here we cannot resolve easily σ for equation 24 because the potential distribution ϕ is a function of the impedance, $\phi = \phi(\sigma)$, as mentioned before, here the ill-posed of the problem can be seen, this by observing or knowing the diffusive behavior of electricity, plus the inherent measurement errors.

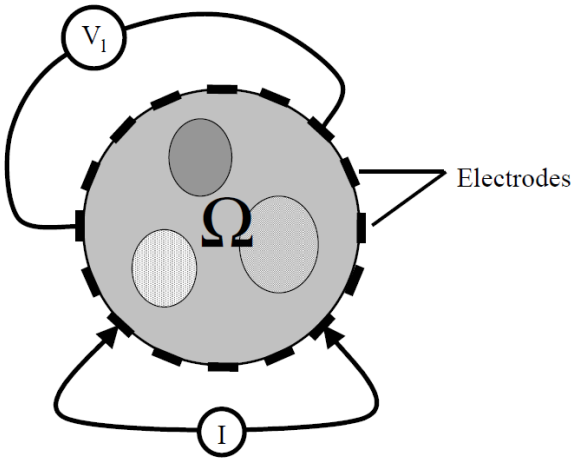

Figure 12: Vessel with object of study Ω, there are 16 electrodes around the vessel, I represents the current injected, and V_1 the voltage measurements, Ω represents the sample core. taken from (Molinari, 2003).

2.3. Function diagram of an EIT system

In Figure 13 a general function diagram of an EIT system is shown, this general representation has 5 main features:

- A screen: This is the display of the image reconstruction result, were the user may obtain information and therefore make conclusions about the object of study.

- Computer and image reconstruction software: This is the device that will be used to perform all mathematical algorithms to make the image reconstruction, it also may govern the data acquisition system or simply may receive data from it.

- Data acquisition subsystem: This part will perform all set of measurements, it is programmed to make all the measurements and it may govern the multiplexer connection stage, it is important to be noted that this data acquisition system may be configured and controller by the computer.

- Multiplexer connection stage: This is a set of multiplexers of different channels, depending on how many electrodes will be used in the vessel, this stage is connected to all electrodes in the vessel and it is used to redirect current or voltage paths to make all necessary measurements to perform EIT, this stage is controlled by the data acquisition system, but may be also controlled from the computer.

- AC constant current source: This is the device that will generate the desired current that

will be injected to the electrodes, it can be governed by the data acquisition stage or directly from the computer.

- Test vessel: The vessel will contain the desire object of study, and in its boundary will have the amount of electrodes desired or configured, the more electrodes it has, a better image may be reconstructed and also a more complex electronics will be required.

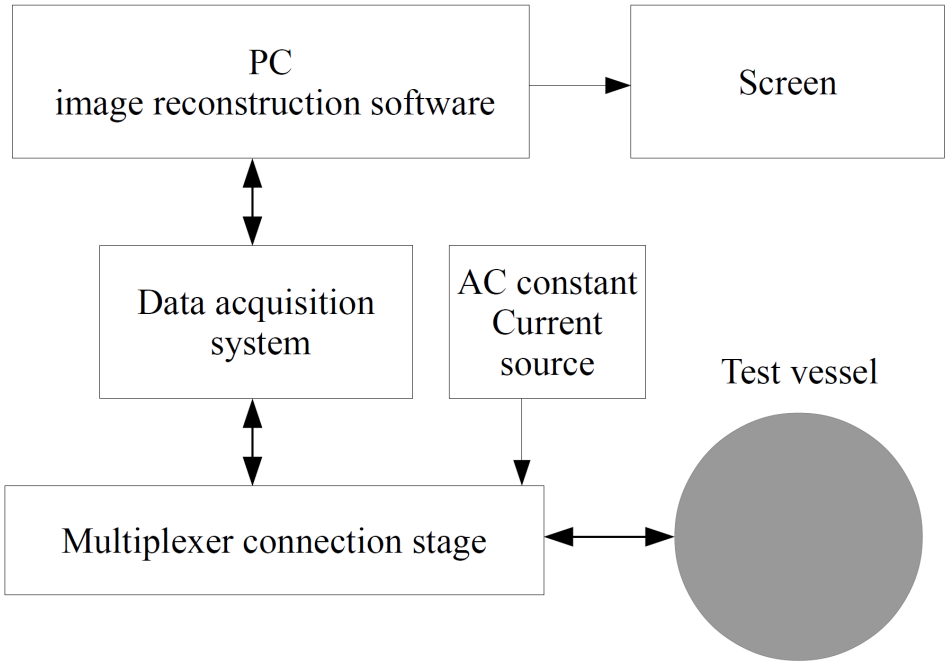

Figure 13: General diagram of an EIT system.

2.4. Methods of simulations and measurements for EIT

Electric impedance tomography requires current to be injected to the medium in study, this current must be constant, in order to have the same current value and a voltage measurement value, to correctly calculate the impedance. The current injected is the stimulation, when injecting current to the medium or stimulating a series of voltage measurements are performed in the medium through the electrodes, it must be noted that the electrodes may inject current or read voltage, depending in which configuration are connected, this different configurations are called methods. There are four main methods, the adjacent drive method, the opposite method, the cross method and the trigonometric method.

2.4.1. Adjacent drive method

The adjacent drive method is also known as the neighboring method, is the most used and common current driven pattern, in Figure 14 there are two main circles that represent the medium of study, this circle is a vessel which contains conductive water, to understand this method its steps are described:

In Figure 14 a), a current injection is applied between electrodes 1 and 2, the current injected in this electrodes generates a flow of electrical current in the medium which is conductive water, circular lines can be seen in the image, this lines represent the current distribution. The first step of the method is to inject the current as mentioned before through electrodes 1 and 2, then an adjacent voltage measurement is performed, this by alternating connections that leads to the system voltmeter, as seen in the picture, there are voltage measurements between electrodes 3 and 4, then 4 and 5, then 5 and 6 and continues until it reads all adjacent voltages finishing in electrodes 15 and 16, once all 13 measurements are performed, electrodes that receive the current injection will change, this is shown in Figure 14 b), now the current injection is between electrodes 2 and 3, this as well will generate a flow of electrical current in the medium, and now a complete set of measurements is made again to the adjacent electrodes, this process is repeated until all pair of electrodes receive the injected current, and all possible adjacent measurement are made, it is important to note that voltages measurements are not made in the electrodes that are being used to inject current as shown. (Harikumar et al., 2013).

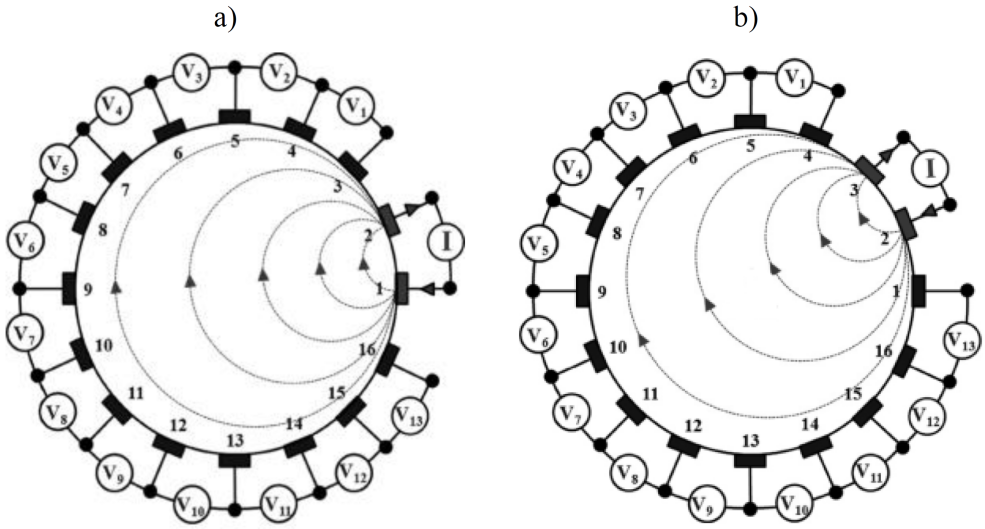

Figure 14: Adjacent measurement or neighboring method, a) First set of measurements while injecting current between electrode 1 and 2, b) Second set of measurements while injecting current between electrode 2 and 3, taken from (Harikumar et al., 2013).

2.4.2. Opposite method

The opposite method also known as polar drive pattern, is commonly used in brain EIT, to understand this method its steps are described:

In Figure 15 a), a first current injection is applied to electrodes 1 and 9, note that this electrodes are placed at 180° apart, the voltage measurements are made to the remain electrodes, 13 voltage measurements are made for each current injection, in Figure 15 b), a second current injection is made, by advancing 1 electrode counterclockwise, now electrodes 2 and 10 are connected to the constant current source, and the voltage measurements are made to the rest of the electrodes as shown. This process is repeated until all pair of electrodes that are 180° apart have had connected the constant current source. This method has the disadvantage that for the same number of electrodes than the adjacent method, only has half of available current injections, although it offers a better distribution of the sensibility, as the current travels with greater uniformity through the imaged body, this means that the opposite method is less sensitive to the boundary conductivity changes, the opposite method as in the adjacent method offers yields 208 measurements (Harikumar et al., 2013).

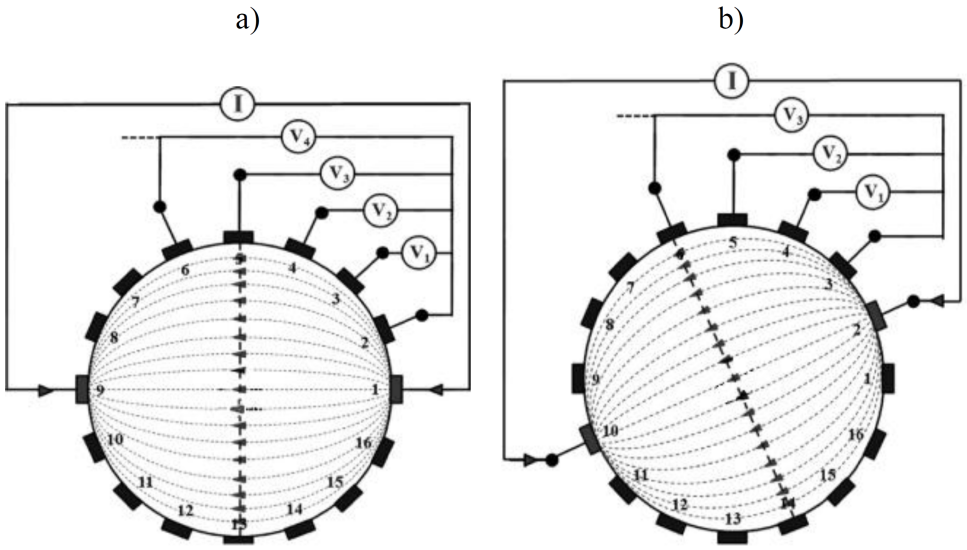

Figure 15: Opposite or polar drive pattern method, a)First set of measurements while injecting current between electrodes 1 and 9 (180° apart), b)Second set of measurements while injecting current between electrodes 2 and 10 (180° apart), taken from (Harikumar et al., 2013).

2.4.3. Cross method

The cross method also known as diagonal drive pattern is not commonly used, to understand this method its steps are described:

In Figure 16 a), the current is injected through electrodes 16 and 2, this method uses electrode number 1 as reference to make the voltage measurements, once the current is injected between electrodes 16 and 2, 13 voltages measurements are made using electrode 1 as reference, the next step shown in Figure 16 b), consists in now inject current between electrodes 16 and 4, electrode 1 remains as reference and all 13 voltage measurements left are made, for the next steps, the combination of connection of the constant current source is through electrodes 16 and 8, 16 and 10, 16 and 12, 16 and 14, hence, the entire measurement procedure yields $7 \times 13 = 91$ measurements. The first stage is made, now the entire procedure is repeated, this time electrodes where the constant current source will be applied are electrodes 3 and 5, 3 and 7, 3 and 9, 3 and 11, 3 and 13, 3 and 15, 3 and 1, this time electrode 2 will be the reference to all voltage measurements made, this stage yiels to another $7 \times 13 = 91$ measurements, for a total of 182 measurements. This method does not have a better sensitivity in the periphery as the adjacent method, but has a better sensitivity all over the entire region

(Harikumar et al., 2013).

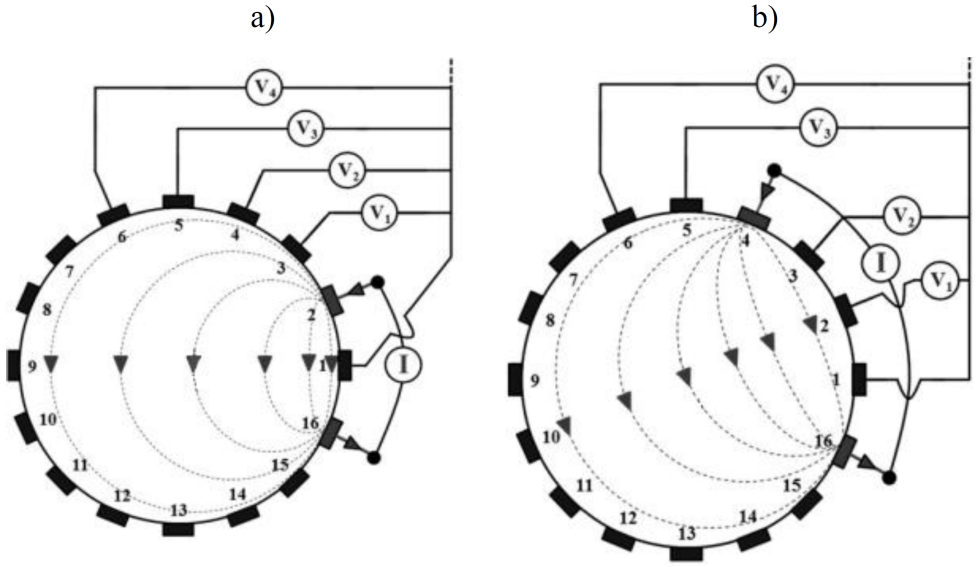

Figure 16: Cross or diagonal drive pattern method, a)First set of measurements while injecting current between electrodes 16 and 2, b)Second set of measurements while injecting current between electrodes 16 and 4, taken from (Harikumar et al., 2013).

2.4.4. Trigonometric method

(Gisser et al., 1987) proposed a current injection method called the adaptive method or trigonometric method, unlike the previous measurements methods, this method injects current and all electrodes and voltages are measured on all electrodes, because current flows through all electrodes at the same time, it needs as many current injectors as the number of electrodes, hence for a 16 electrodes system, it will require 16 current injectors, this electrodes can be fed from -I to +I, to allow different current distributions. For this method, the boundary voltages are measured with respect to a single grounded electrode, so for a 16 electrode system, this method will produce 15 voltage measurements, once this is made, the current projection is rotated to one electrode increment, now new measurements are made, as result is yields to a total of $8 \times 15 = 120$ independent voltage data, the main problem of this method is the number of the current drivers, and the unknown contact impedance that will affect on the reconstruction algorithm (Harikumar et al., 2013).

2.5. Variations in Electrical Impedance Tomography

EIT has different approach, when studying an object and taking data to perform an image reconstruction EIT will be known as absolute EIT. But if the EIT is continually made in an object, tissue or something else, now it will be known as difference EIT, because now there are data taken in different times. Typically frequencies of 10 to 100kHz are used, when making EIT at different frequencies it is known as multi-frequency electrical impedance tomography.

2.6. Applications of Electrical Impedance Tomography

2.6.1. Lung

EIT is useful for lung monitoring, it has high absolute contrast of the lungs because lung tissue impedance is higher than other tissues. Lung impedance changes when inspiration and expiration, this is one of the main reasons that one of the most promising clinical applications of EIT is in lung monitoring.

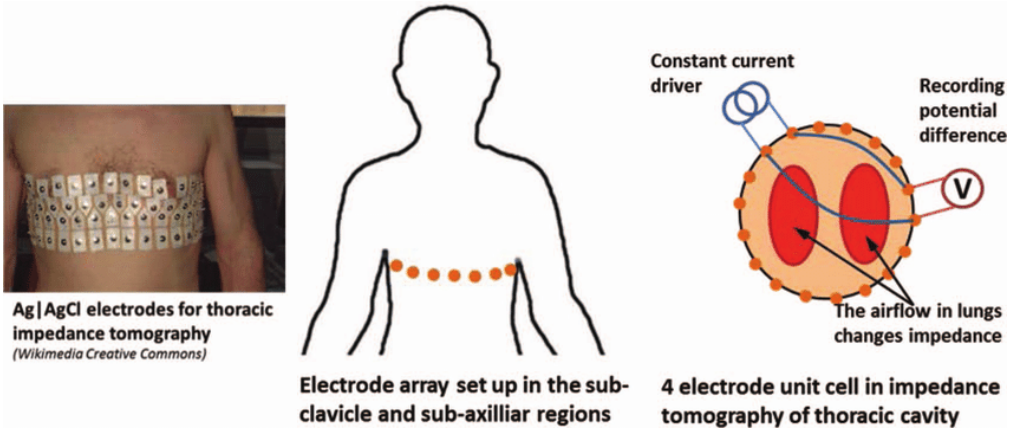

Figure 17: Electrical Impedance Tomography (EIT) of thoracic cavity to lung function, taken from (Rai et al., 2013).

2.6.2. Breast and Cervix

Electrical properties between normal and malignant breast tissues differ, this allows to detect possible cancer in breast through determination of electrical properties of the breast. Researches around the world agree in using a frequency sweep of EIT (multi-frequency impedance tomography) to detect possible breast cancer. For cervix, the principle is the same, also not only detecting but predict cervical intraepithelial neoplasia (CIN) grades 2 and 2

best known as Cervical cancer according to the Papanicolaou test with a sensitivity and specificity of 92 % each.

2.6.3. Brain

EIT has been also studied for brain imaging to detect brain ischemia, hemorrhage and several other pathologies associated with impedances changes due to cell swelling.

2.6.4. Overview

Also applications in material engineering has been made, the EIT technique has been used to estimate the conductivity distribution of a conductive polysilicon this for semiconductor manufacturing. Nanotechnology also has had EIT applications in carbon nanotube (CNT) imaging, it has been useful to develop multifunctional CNT-based sensing skins. In civil engineering EIT has been useful in leak detection or damage detection in buried pipes (Bera, 2018). Although EIT has 4 decades of research it has only medical applications for lungs, useful for diagnoses and in ventilator monitoring, other medical applications remain in research, there has been many advances that prove that the use of EIT in medicine will be certain to happen, it is necessary that research continue, not only in hardware or software but also in applications in humans, in order to ensure its certainty and reliance.

2.7. EIDORS library

EIDORS acronym means: Electrical Impedance Tomography and Diffuse Optical Tomography Reconstruction Software Adler and Lionheart (2006), basically is a compendium of algorithms to be used in medical and industrial applications, all software from EIDORS is free and open to change, make, promote and contribute its contents, it can be used in Matlab version above 2016b or 9.1 and in Octave version above 4.4, it is licensed under the GNU (General Public License), it contains examples and tutorials to be used. Most of its contents has been developed for EIT, it was released in 1999, its origins come from a Ph.D thesis of Marko Vauhkonen and the work of his supervisor Jari Kaipio at the university of Kuopio. The EIDORS library has been used in many EIT projects and continues to be an essential tool for EIT.

Chapter III

3. System development

The proposed EIT system, generates an image from a test unit, which consists of a circular vessel with a conductive liquid (water with potassium chloride or sodium chloride), where the object under test is entered, then 16 electrodes are connected to several multiplexers and a MCU, which allows the impedance mapping of the object under test or body to measure and characterize to form its image.

Figure 18 shows the physical aspect of the test unit (vessel) used in this Ph.D thesis to test and validate the proposed EIT system. It consists of an impedance acquisition subsystem that sends through USB port the impedance measurements values to a SBC-RPi4. Then, the RPi4 after receiving the data stream, executes the well-known EIDORS Adler and Lionheart (2006) library for the image reconstruction. The shape of the sample measured must be known in order to verify the correct image reconstruction, this is also helpful to calibrate the image reconstruction algorithm and therefore, to obtain a better image approximation. There are many mathematical models depending on the shape of the test unit (vessel), for this work a circular shape was used.

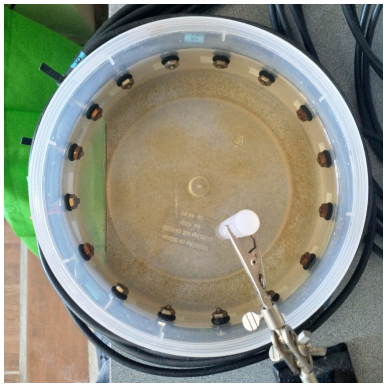

Figure 18: Test unit (vessel) with 16 stainless steel of 304-caliber electrodes.

3.1. Adjacent measurement method

In this Ph.D thesis, the adjacent method for electrical impedance tomography is used (better explained in 2.4.1), it consists in applying a known current to an electrode pair, where these electrodes are neighbors, once the known current is applied through these electrodes,

an adjacent voltage measurement is made in all the next connections of the cylinder water tank (vessel).

Figure 19 depicts how a constant current source is applied on two neighbor electrodes, then, a voltage measurement of the remaining pairs is performed, then, by means of a multiplexer, the voltage source is connected to the next electrode neighbor pair and the adjacent voltage measurement is made again until covering all the combinations, in this case, for a 16 electrode base, there are 208 measurements.

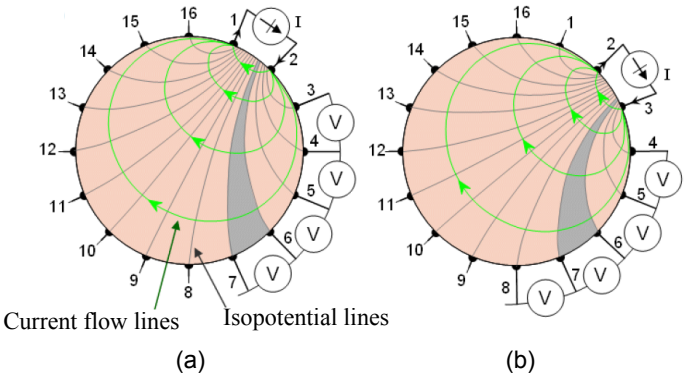

Figure 19: Adjacent measurement method, taken from Calvo Hernando (2018). (a) First measurement process, the current is injected between electrodes 1 and 2, (b) Second measurement process, the current is injected between electrodes 2 and 3.

3.2. Test unit (vessel)

Figure 21 depicts the test unit, it is a round-shaped plastic vessel, which is used to contain the experimental samples (salty water, metal, plastic objects, fruits, etc.), then 16 stainless steel 304-caliber are used as electrodes for the proposed EIT system, which are placed equidistantly, these screws are introduced in the plastic vessel using nuts and rubbers to prevent leakage. This vessel is used for all the experimental procedures of the proposed system, attached to each electrode, a shielded cable is used to connect to the electronic system in order to prevent noise. The 16 electrodes of the vessel are enumerated counterclockwise, and are connected to the three ADG1406 multiplexers, so the MCU manages their connections to perform the required measurements.

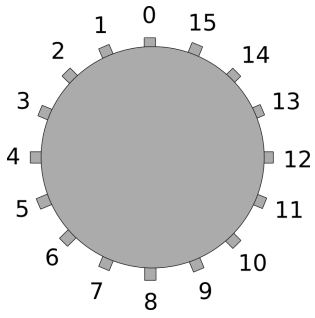

Figure 20: Test unit with 16 electrodes, counterclockwise enumerated.

3.3. Electronic design

Figure 21 depicts the block diagram of the proposed EIT system. The hardware consists of a data acquisition (DAQ) subsystem and a user interface. The DAQ subsystem hardware was coded to employ the adjacent measurement method (subsection 3.1) on the test unit. The Arduino MCU selects which pair of electrodes is connected to the AC constant current source, and the other pair that is connected to the adjacent electrodes. Then the signal is processed with the help of an instrumentation amplifier configured as a peak detector connected to an ADC that sends the voltage measurement value through an SPI (serial peripheral interface) protocol by receiving commands from the Arduino MCU, which sends the raw data through serial communication at 500000 bps to a central processing unit (CPU), e.g. the RPi4, as is the case here.

Table 1 shows the system's features, the proposed EIT system works with 110 V_{AC} at 60 Hz, the peak power consumption is 15 W, it has three DC operating voltages, 5 V, 12 V and -12 V, one MCU Arduino Mega 2560 to manage the data acquisition, the communication between MCU and RPi4 is via USB 2.0 port configured at 500000 bps, the ADC part number is ADS1256 with 24 bit resolution at 30 kSPS, it has four multiplexers ADG1406 to access 16 electrodes, input frequency range 4-80 kHz, the frame rate is 12 per minute and the diameter of test unit is 17.5 cm.

H

Table 1: Proposed EIT system features.

Description	Feature
Electrical connection	$110V_{AC}$ 60Hz
Peak power consumption	15 W
Embedded voltage source	5 V, 12 V and -12 V
MCU	Arduino Mega 2560
Communication	Serial USB 2.0
Communication speed	500000 bps
ADC	ADS1256 24 bit resolution at 30 kSPS
Multiplexers	Four 1 to 16 decoder ADG1406
Number of electrodes	16
Input frequencies	$4 - 8$ kHz
Frame rate	12 per minute
Connectivity	Bluetooth & USB 2.0
Networking	Ethernet & WiFi
Test unit diameter	17.5 cm

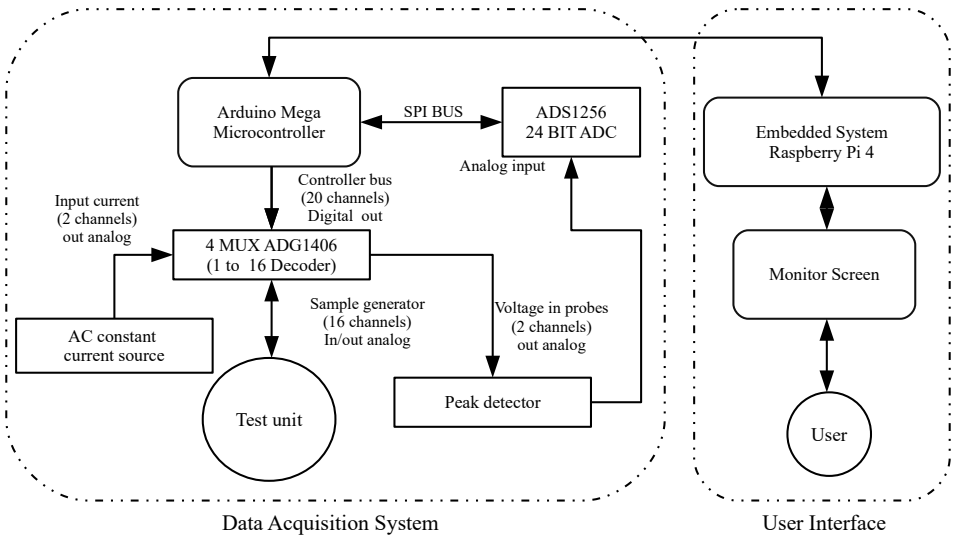

Figure 21: Block diagram of the proposed EIT system. (a) Data acquisition stage, (b) User interface.

3.3.1. Constant current source

To develop the AC constant current source the ICL8038 precision waveform generator was used. This because it is a monolithic integrated circuit capable of generating high accuracy sine, square, triangular, sawtooth and pulse waveforms with a minimum of external

components. The frequency can be selected externally from 0.001 Hz to more than 300 kHz. In this paper, the constant current source applied to the proposed EIT system consists of an AC voltage source at 2.56 Vpp, with a frequency of 4 kHz and 40 kHz for the reported tests. This AC signal is injected into a circuit that converts the voltage into a constant current source. Figure 22 depicts the proposed circuit of the constant current source, which consists of an array of resistances, a TL084 operational amplifier, and the 2N3906 PNP transistor. The voltage in pin number 3 of the operational amplifier remains fixed because of the high impedance, and pin number 2 shares virtually the same voltage value. When any load is connected between pin CSp_1 and CSp_2, the voltage in pin 2 maintains its value, and the transistor Q1 delivers the necessary current to the load; the maximum current is the voltage in pin number 2 divided by the resistance R_4. The current Is is calculated by (25) and the value for the experiment is 91,42 μA with $V_p = 2{,}59$V.

$$Is = (R_2)(\frac{V_p}{R_2 + R_1})(\frac{1}{R_4}). \tag{25}$$

The pins CSp_1 and CSp_2 are connected to the four analog multiplexers ADG1406. These pins are now an AC constant current source, which is applied on the test unit for the proposed EIT system. The constant current source sensitivity to load changes is shown in Figure 23 and its values in Table 2. The voltage yields to the saturation value in the TL084 op-amp when the load exceeds 120 $k\Omega$; therefore, this is the limit for the fixed current source at the proposed voltage. The load used in the system test is below 120 $k\Omega$ and therefore the constant current source works properly.

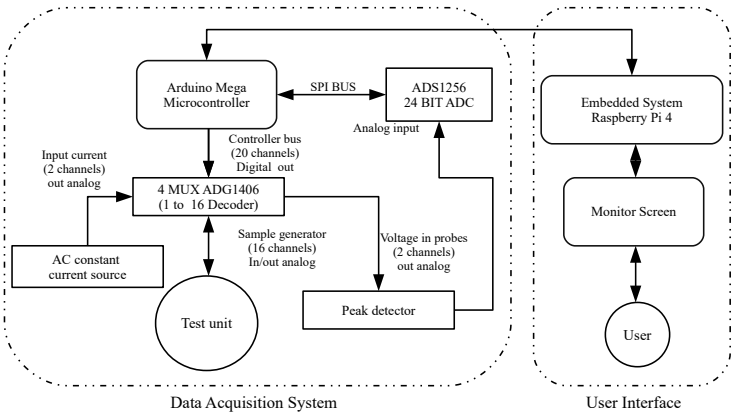

Figure 22: Constant current source circuit is 91,42 μA.

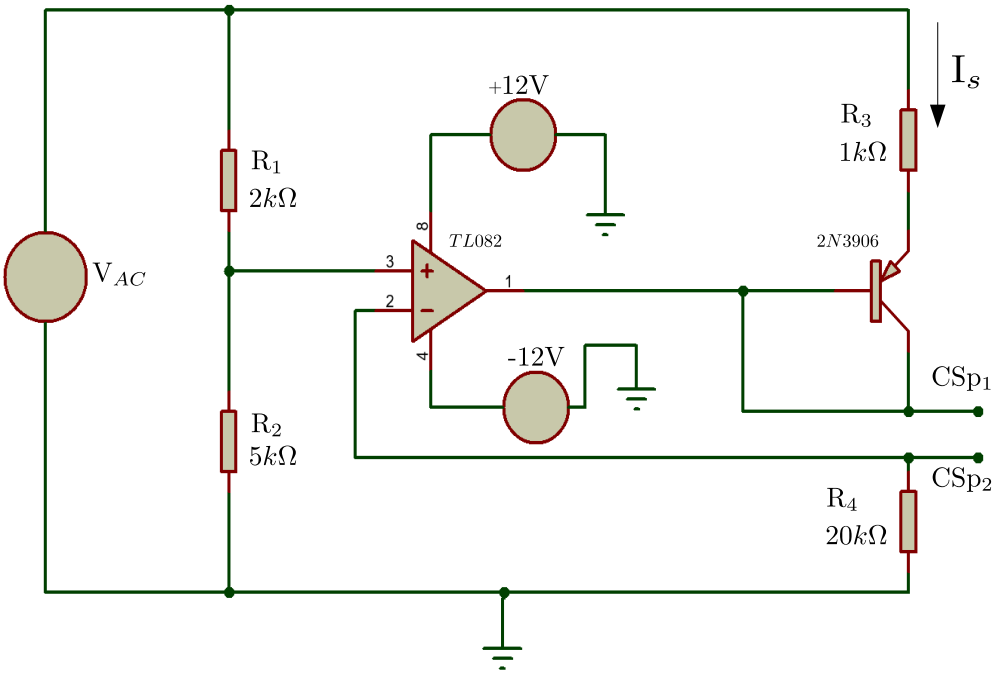

Figure 23: Output current sensitivity to load impedance changes: (a) from 0 to 120 kΩ the current remains fixed at 91,42 μA, a higher impedance value falls out of the fixed current range; (b) the voltage in CSp_1 yields to voltage saturation of the TL084 op-amp when the load is higher than 120 kΩ.

3.3.2. CMOS multiplexer

The ADG1406 is a CMOS multiplexer that can be used in biomedical applications like EIT. Internally, it has a decoder that connects input/output pins S_1 to S_{16} to an input/output pin D, with a resistance of only 9.5 Ω and a maximum current flux capacity of 300 mA. By using 4 multiplexers, it is possible to connect four different probes to 16 different outputs, this configuration makes the adjacent current injection and adjacent voltage measurement in the test unit possible. Two probes are used for the AC constant current source and the other two for the voltage measurements. If a higher number of electrodes is required, the number of multiplexers has to increase, i.e., 8 multiplexers are required for a 32-electrode EIT system, as well, minor changes in the hardware and software have to be performed.

3.3.3. High-precision peak detector

A peak detector is a circuit that takes the maximum voltage value of an AC voltage signal (V_p), and it maintains it for a finite time duration, it is composed of a diode connected to a

Table 2: Measurements for output current sensitivity to load impedance changes test.

Load value [Ω]	Current Amplitude [μA]	$VCS_{p_1}[V]$
0.109377	91.4262	1.828
1500	91.4262	1.965
15000	91.4259	3.199
30000	91.4256	4.571
45000	91.4253	5.942
60000	91.425	7.314
75000	91.424	8.685
90000	91.424	10.05
105000	91.424	11.42
120000	91.423	12.79
135000	86.333	13.42
150000	79.134	13.45
200000	61.24	13.47

capacitor and a resistance that discharges the capacitor because of the peak variation. For this EIT system, a high-precision peak detector was used. Figure 24 depicts the proposed high-precision peak detector circuit. The pin from the MUX, which corresponds to a voltage measurement on the test unit (vessel), connects to the high-precision instrument amplifier AD620 from Analog Devices. The gain is set to approximate 1.5 and the output is then passed through C_1, which allows only AC current, thus eliminating the offset signal. The signal is then applied to an operational amplifier LM2903, which is a dual comparator. Pin 7 is connected to a diode and a voltage is applied to the capacitor C_2 and resistances R_{12} and R_{13}. Then an MCP601 operational amplifier was connected as a voltage follower, and was chosen on the basis that its characteristics mean it is very often used for data acquisition. Its feedback goes to the LM2903 comparator, this configuration delivers a peak voltage for the signal input; pin 6 of the MCP601 corresponds to this peak and is connected to the ADC.

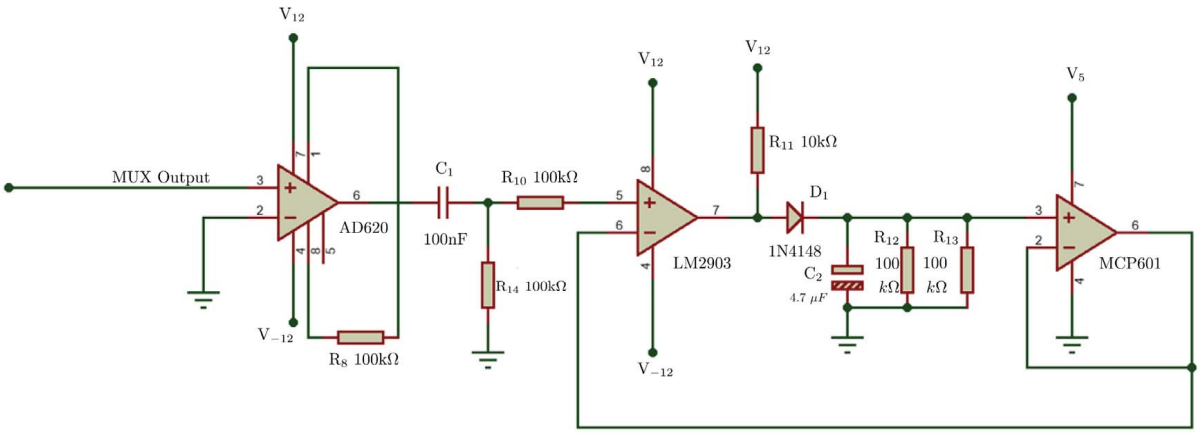

Figure 24: Proposed high-precision peak detector.

Figure 25 shows the peak detector output measured with an oscilloscope. The pink horizontal line represents the detected peak voltage level.

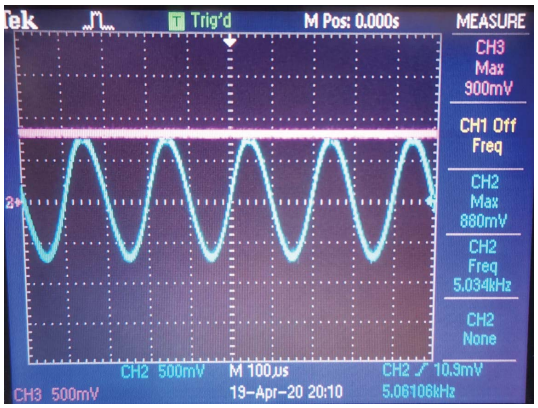

Figure 25: Peak signal detected by the high-precision peak detector.

3.3.4. Analog-to-digital converter (ADC)

Once the signal is conditioned from the test unit (vessel) through the multiplexers and peak detector, the signal is applied to ADS1256, which has very low noise, 30 kSPS of 24-bit resolution, and 8 analog input channels. It has several applications including in biomedical, testing, and measurement equipment. This ADC is connected through an SPI communication protocol and works as a slave to an Arduino MCU, which controls the voltage measurements.

3.4. Firmware and functions for the proposed EIT system

The following algorithms are responsible for acquiring data to reconstruct an image. The steps are as follows: Data is processed through a statistical algorithm in the MCU and the resulting average data values are received through a serial port from an MCU to Matlab (PC test) or RPi4 (SBC test), a complete measurement cycle is continuously received, and after each cycle is received, data is compared with the calibration data file through the comparison algorithm. The final data and the calibration data are processed with the image reconstruction software (EIDORS) Adler and Lionheart (2006) and a real-time reconstructed image is created.

3.4.1. Data acquisition firmware

The data acquisition firmware enlisted in Algorithm 1 is embedded in the Arduino MCU and may be coded on different MCU devices. Important features include a baud rate of 500000 bps, the adjacent method routine in the main while loop, the voltage measurement algorithm by means of an ADS1256 and the statistical mean that is calculated to determine the best value of each voltage measurement. In Algorithm 1 the acquisition process is described, the pseudo code used for this algorithm consists in various steps. First the main libraries to make the ADC work are called, then the parameters to control the multiplexers are set, the communication is set to 500000 bps, and the library to communicate through SPI is called and the ADC is initialized. An infinite loop that will be taking cycles of voltage measurements using the adjacent method is started, 250 samples are taken for each voltage measurement. As described, the Algorithm 1 selects the pair of electrodes to inject current, and then the electrodes to make voltage measurements (ADC sends values through SPI communication to MCU), once the 250 samples are taken, the Data Acquisition Algorithm 1 discards the first 130 voltage measurement values that correspond to the transitory state of the voltage measured, then the mean is calculated for the rest of the voltage values, generating a unique average value which is send as raw data through serial communication to RPi4, the process is continuously repeated.

Algorithm 1 Firmware for Data Acquisition

```
include SPI.h                                          #Library to communicate with 24 bit ADC ADS1256
include digitalWriteFast.h                             #Library to communicate with 24 bit ADC ADS1256
Define all digital output channels to control 4 decoders
Begin serial communication at 500000 bps
Begin SPI library
Initialize 24 bit ADC ADS1256
While(true)                                            #repeat indefinitely
    Set parameters to sample measurements in test unit #Number of samples (250), number of electrodes (16)
    While(n = 0, n < 16, n++)                          #Cycle to perform the adjacent voltage measurement method
        Select pair of probes to inject current
        While(m = 0, n < 12, m++)                      #Cycle to perform the adjacent voltage measurement method
            Select pair of probes to measure voltage
            Take k samples with 24 bit ADC ADS1256     #250 samples set
            Discard first 130 values                   #Values of the transitory state
            Calculate the statistics mean of the rest of the sample vector
            Send the value to serial port as raw data.
            Deselect pair of probes to measure voltage
        End While
        Deselect pair of probes to inject current
    End While
End While
End Routine
```

3.4.2. Firmware for data comparison

The firmware described in Algorithm 2 for data comparison was coded for RPi4 and determines if the data measured in real time differs sufficiently from the calibration data. It calculates if the data collected is different from the calibration data due to the sensibility of the system to noise; even if two data vectors measured from the system look the same, a small difference, even in the order of 1×10^{-15}, delivers a faulty image reconstruction for the object in the test unit (vessel), owing to the ill-posed nature of the problem Dimas et al. (2020); C. Dimas, N. Uzunoglu, P. P. Sotiriadis (2019); Malone et al. (2015); Russo et al. (2017b), as discussed in the introduction. Therefore, the comparison function determines if the acquired data is within a margin of error tolerance. If this is the case, it considers the measured data to be the same as the calibration data; otherwise, it leaves the data without any adjustment for the reconstruction algorithm. An error tolerance of 3 % was chosen because while making measurements, we found a systematic error rate of at least 2 %, due to noise and other physical limitations.

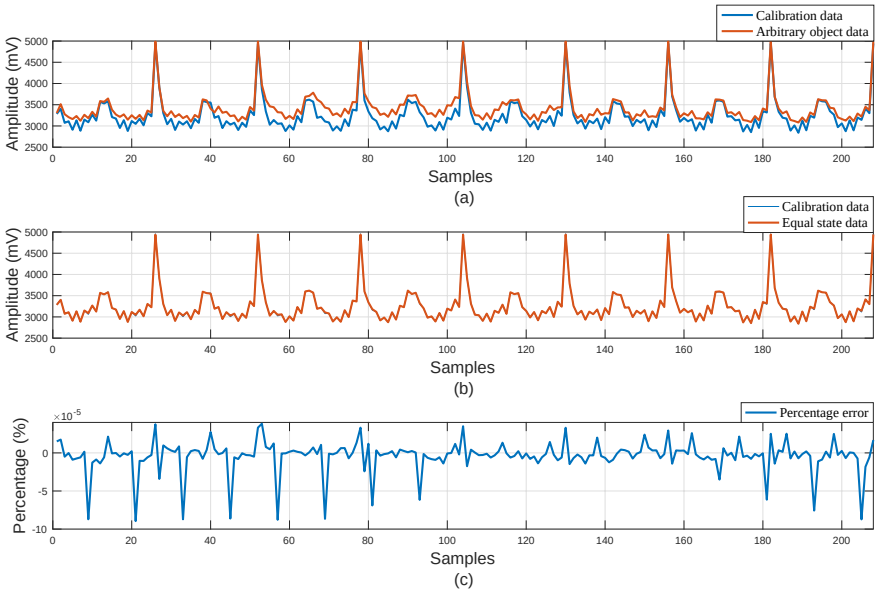

Figure 26: Three graphs of a measurement cycle. (a) Comparison between calibration data and arbitrary object data, (b) Calibration data and second round of calibration-plane measurements, and (c) Percentage of error between calibration data and the second round of measurements.

Figure 26 shows three graphs. Graph (a) shows calibration data and data from arbitrary measurement of an object. Graph (b) shows two measurements that are almost the same; one is calibration data and the other is a measurement of the system in the same state as the calibration plane (second round of calibration-plane measurements), which physically means that it is a measurement with the test unit (vessel) with only salty water. It is clear from graph (c), which shows the differences between the two measurements, that they are practically the same. Should the reconstruction algorithm receive this, it will discard the data measured and consider it to be the same as the calibration data. Algorithm 2 describes the pseudo-code for this function, the function receives two data vectors, an n tolerance value and a timeouts value to determine whether the vector are or not practically the same, each vector value is compared, and if it outside an n tolerance value, a flag variable is increased and if it overpass the timesout value set, then vectors are not the same, and therefore not changed, however if it does not overpass the value set, then vector A becomes equal to B meaning that both vectors are practically the same.

Algorithm 2 Firmware for data comparison

```
vector A, vector B, n, TimesOut                                  #Receive two vectors of same size and parameters
for k=1 to length A, Flag=0                                      #Compare if vector A=B at n % tolerance
        if A(k)¡(1-n/100)*B(k) or A(k)¿(1+n/100)*B(k)            #Checks if the value is outside the n % tolerance value
                Flag=Flag+1                                      #Flag value increases every time is outside the n % tolerance value
        End if
End for
if FlagTimesOut      #Determines if the vector is inside the n % tolerance value
        A=B          #The function considers that the vector is the same because is inside the n % tolerance value
return A             #Returns the vector A, being different or equal to B depending if is inside the n % tolerance value
```

3.4.3. Function for statistical analysis

The Statistical Function enlisted inside Algorithm 1 performs statistical calculations with the acquired data to be smoothed, due to the ill-posed nature of the problem Dimas et al. (2020); C. Dimas, N. Uzunoglu, P. P. Sotiriadis (2019); Malone et al. (2015); Russo et al. (2017b). This makes it possible to determine which measurement is the best value for use in the image reconstruction process. The adjacent method was described in section 3.1. It consists in taking measurements using adjacent electrodes in the proposed EIT system. In this paper, 16 electrodes were used, and therefore, 208 different measurements can be obtained from the test unit (vessel). Each measurement is acquired by using an ADS1256 ADC through the acquisition of $n = 250$ samples, which means that n can be changed in order to improve accuracy in each data acquisition process.

Figure 27 depicts four graphics of the 250 samples that are performed for each voltage measurement. A transient behavior can be observed in the measurements. For this reason, the statistics mean, median, and mode were calculated for each vector of samples. Several experiments were performed and it was found that the mean and median are enough similar, though the median is more accurate with respect to the actual measured voltage considering all 250 raw value samples, the mean represents a lower computational cost and an acceptable average value, added to this, to improve its accuracy, the first 130 samples are not taking in account. This means that for every voltage measured, the mean is calculated to define the best value for the last 120 samples resulting in an improved mean average value with low computational cost. This process is repeated 208 times to perform a complete adjacent measurement cycle in the proposed EIT system, and it takes 4 seconds to complete a full voltage scan for 250 samples per measurement.

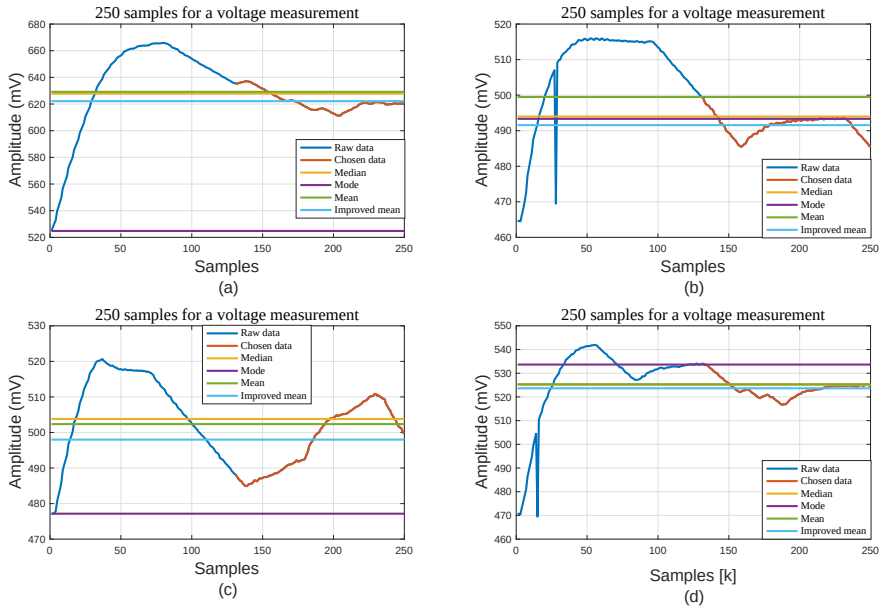

Figure 27: Four graphics showing measurements for four different electrode pairs, taken with the proposed EIT system by acquiring 250 samples. A transient voltage behavior is observed. (a) First pair of electrodes, (b) Second pair of electrodes, (c) Third pair of electrodes, and (d) Fourth pair of electrodes.

3.4.4. Firmware for calibration and real-time working

The firmware for calibration and real-time working enlisted in Algorithm 3 was coded for RPi4 and has two main features. The first one is a calibration routine, which executes an adjacent measurement routine in the test unit (which the intrinsic errors of the electrodes and cables are considered, such as: lift-off, parasitic resistances, inductances, capacitances, corrosion, noise levels, etc.) when it contains only conductive water. Once finished, it creates a file with the raw data from the test unit with only conductive water. This data is the calibration data (data to be applied in the reconstruction algorithm). The second feature is the fact that it performs an adjacent measurement routine in real time for data acquisition for the test unit (vessel). Once a measurement cycle is completed, it performs the reconstruction algorithm for EIT using the EIDORS library. The calibration function uses the acquired data in real time and the calibration data measured in the calibration process, resulting in a real-time reconstructed image from the impedance mapping in the test unit (vessel). Algorithm 3 describes the general pseudo-code routine for the calibration and real-time system features. If the user decides to calibrate the system, then a single measured cycle is received from the

MCU and stored in a calibration file (file 2), and then it closes the communication. Once the user has a calibration file, the real-time feature can be used by setting the calibration flag to 0, now the system will receive data from the serial communication and will store it in a real-time data file (file 1), the values received are 208, which correspond to a complete voltage measured cycle. Once the real-time file is created, the function reads both real-time and calibration data files, it performs the function for data comparison (algorithm 2) then the image reconstruction function is called and a real-time reconstructed image is showed on-screen, the process is repeated until the cycles decided by user are finished.

Algorithm 3 Firmware for calibration and real-time working

```
Set parameters as in acquisition system and operation frequency
Read calibration flag (true or false)                    #0 determines real-time mode, 1 determines calibration mode
Open serial communication, (set COM number) at 500000 bps
Open txt files according to parameters                   #files to save calibration or real-time data
Begin serial communication at 500000 bps
While(Total loops)                                       #Repeat until loops set by user
    While(value¡208)                                     #Repeat until cycles wanted by user settings
        Read COM buffer
        Save to file 1                                   #Saves the data received into a file named 1
        if calibration true
            Save to file 2                               #Also saves a file for calibration data in a file named 2
        End if
    End While
    if calibration false
        Read data from file 1 and 2                      #Read real-time(file 1) and calibration data(file 2)
        process Algorithm 2 between files                #Calibration data and real-time data files
        Call reconstruction image function (Algorithm 4)
        pause system for .1 second                       #Allows the system to update the reconstructed image
    End if
End While
Close serial port communication
End Routine
```

3.4.5. Image reconstruction

The EIDORS library Adler and Lionheart (2006) was used to perform image reconstruction from the collected data. We decide to use EIDORS because we find that its good performance has been proven in the literature Ansory et al. (2018); Kusche et al. (2015),

furthermore, this works correctly in Matlab or GNU Octave, has a lot of feedback and is easy to implement on EIT systems. According to the library instructions, many configurations are possible; for this research, the settings used were the following: a 2D circle model with 16-electrode configuration, no measurements on current-carrying electrodes, rotation of measurements with stimulation pattern, adjacent current injection, adjacent voltage measurements, and the number of rings set to 1 (however, when using 2D reconstruction, this parameter is disregarded by the software). Two vectors of 208 values must be introduced into the reconstruction function - data at earlier time and data at later time - in order for the reconstructed image to be shown on screen. Algorithm 4 describes the image reconstruction function. The function receives parameters of number of electrodes, real-time(data at later time) and calibration data(data at earlier time). The EIDORS library functions are called, the configuration is described in the algorithm, and this configuration was chosen according to the system developed, taking into consideration the shape of the vessel, number of rings (which corresponds to 1 ring), the number of layers (this number is disregarded as it is only needed for 3D reconstruction but necessary to make the function work), the number of electrodes (which is 16), the options (no measurement on current carrying electrodes and rotate measurements, this was set according to the adjacent measurement method). The first "{ad}" parameter corresponds to the way of injecting current, which is adjacent current injection, and the second "{ad}" parameter in the algorithm code, corresponds to the way of making the voltage measurements which is adjacent voltage measurement, in other words, these parameters tell the function that the adjacent measurement method is applied to inject the current and to make the voltage measurements. The current parameter may vary and this helps to have different approaches of the reconstructed image and is set to 1, the rest of the code is needed to solve the inverse problem, and to finally show the reconstructed image on-screen.

Algorithm 4 Image reconstruction

```
1: electrodes=16, real_time_data, calibration_data, current    #16 electrodes, real-time and calibration data, current set
2: imdl = mk_common_model(c2c2,electrodes)                     #c2c2 corresponds to a circular vessel, generates the model
3: fmdl = mk_circ_tank( n_rings , three_d_layers, n_electrodes)    #parameters for the model
4: options = {no_meas_current,rotate_meas}                     #options set according to adjacent measurement method
5: [stim, meas_select] = mk_stim_patterns(configuracion,1,{ad},{ad},options,current)    #Settings according method
6: imdl.fwd_model.stimulation = stim                                  #function to create model for stimulation
7: imdl.fwd_model.meas_select = meas_select                           #function to create model for measurement
8: img = inv_solve(imdl,calibration_data,real_time_data)              #function that solves inverse problem
9: show_slices(img)                                                   #Shows reconstructed image
10: End Routine
```

Chapter IV

4. Experimental results

4.1. Comparison between the PC and RPi4

This chapter presents a comparison between the proposed EIT system, developed using GNU Octave for RPi4, and an EIT system developed using Matlab for PC. Both forms of hardware apply EIDORS to verify that all numerical computation and application with the RPi4 for the proposed EIT system is competitive with respect to the PC. To perform this comparison, the raw data used for the PC and RPi4 is the same. Data was acquired from measurements from the test unit (vessel) with several objects to characterize their impedances: for example, conductive water only, to establish the zero state or calibration plane; a round metallic recipient, which has high conductivity; and a glass, which has low conductivity. It is also important to mention that all numerical calculations were performed by both types of hardware, and double-precision variables were used according to the IEEE 754 standard Zuras et al. (2008). For a better understanding of the experiments, each configuration with photos is presented to show that the EIT with an RPi4 does not compromise accuracy or effectiveness.

4.1.1. Calibration of the proposed EIT system

Figure 28 shows the test unit (vessel) with only conductive water to perform calibration. First, it was necessary to connect the test unit (vessel) to the proposed EIT system, then execute the function for calibration and real-time working.

Figure 29 shows the measurements for image reconstruction of the calibration plane. The left-hand side shows three graphs processed using Matlab for the PC, representing a cycle measurement, calibration data, and the error (difference) between both signals. On the right-hand side, the same measurements are shown using GNU Octave for RPi 4.

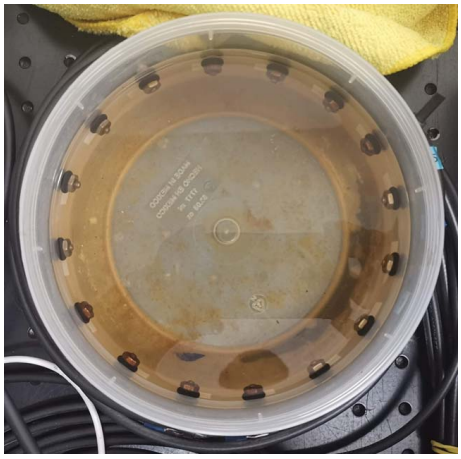

Figure 28: Test unit (vessel) with only conductive water to perform calibration.

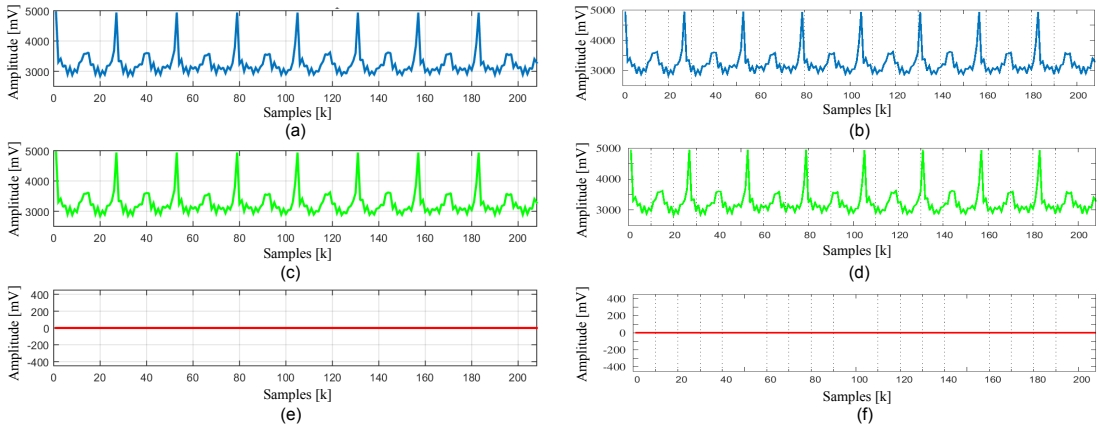

Figure 29: Comparison of measurements for image reconstruction between the PC and RPi4. (a) Measurements corresponding to the calibration plane using the PC, (b) Measurements corresponding to the calibration plane using RPi4, (c) Second round of calibration-plane measurements using the PC, (d) Second round of calibration plane measurements using RPi4, (e) Differences between first and second-round measurements using the PC, (f) Differences between first and second-round measurements using RPi4.

Figure 30(a) shows the image reconstruction for the calibration plane obtained using Matlab on the PC. Figure 30(b) shows the image reconstruction obtained using GNU Octave for RPi4. The reconstructed image achieved is practically the same, and the hardware used was unaffected, proving that RPi4 can be used for EIT.

4.2. Orange as test unit

First, a cycle of 208 measurements must be performed to obtain the calibration data in the actual state of the orange. Another cycle of 208 measurements is then performed and

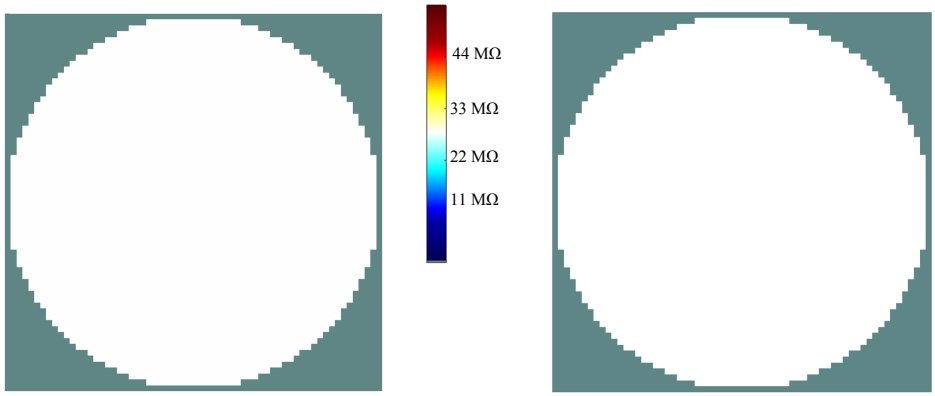

Figure 30: Comparison of image reconstruction for the calibration plane on the PC versus RPi4: (a) Image reconstruction using a 4 kHz signal, with no object inside the vessel and data processing on the PC, (b) Image reconstruction using a 4 kHz signal, with no object inside the vessel and data processing on RPi4.

the result is compared with the calibration-plane measurements. In other words, a complete cycle is performed in the same conditions as the calibration plane. Figure 31(a) shows the orange as the test unit in the calibration plane. Figure 31(b) shows the corresponding image reconstruction: a full white circle is observed, meaning the information is the same as is in the zero state or calibration plane. Figure 31(c) shows the orange as the test unit with seawater injected. Figure 31(d) shows the image reconstruction of the orange with seawater injected; a navy blue salty spot can be observed, where the conductivity of the seawater is higher than the calibration plane, and therefore the navy blue spot represents less impedance than the calibration plane (white). Other color shades can also be seen, such as aqua-green, which shows low filtration of salty water to other areas of the orange. Even yellow is observed, which represents a minor alteration of electrical impedance with respect to the calibration plane. This test shows a potential application in food industry, for example to know the food maturity process and to know when it is going into a state of decomposition.

4.3. Real-time results on RPi4

Figure 32(a) shows a glass object placed inside the test unit (vessel); dark red colors can be observed in the reconstructed image and represent the high impedance of the glass. Figure 32(b) shows a metal object placed inside the test unit (vessel); navy blue colors can be observed in the reconstructed image and represent the low impedance of the metal.

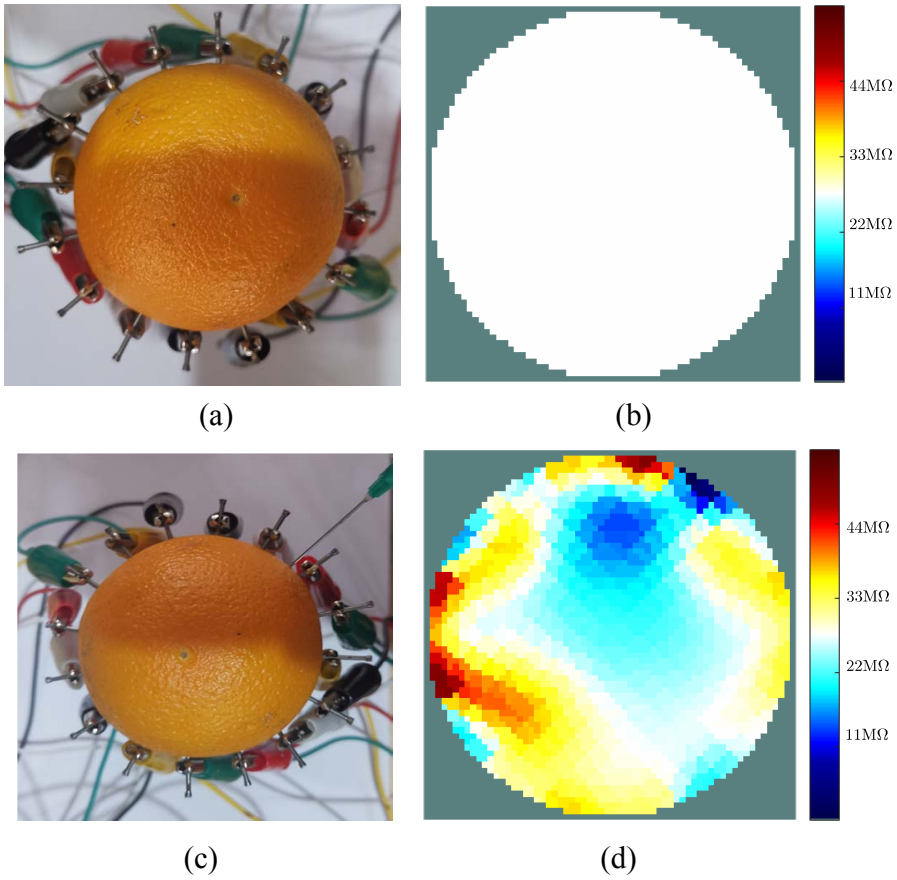

Figure 31: Test of the proposed EIT system using an orange as the test unit. (a) Orange in the calibration plane, (b) Image reconstruction of orange in the calibration plane, (c) Orange with seawater injected, (d) Image reconstruction of orange with seawater injected.

Figure 32(c)-(e) shows a glass and metal object placed inside the test unit (vessel) in different positions; in the reconstructed images, dark red and navy blue shapes can be seen, which represent the impedance of the glass and metal objects, respectively. Furthermore, if the objects move, the colored shapes corresponding to the objects also move. Figure 32(f) shows an orange placed inside the test unit (vessel); in the reconstructed image, a dark red shape can be observed, which represents the high impedance of the orange. As shown in previous reconstructed images by PC and RPi4, it can be concluded that numerical computation and reconstructed images deliver practically the same results. This is because both types of hardware perform numerical calculations according to the IEEE 754 standard Zuras et al. (2008). RPi4 has ample hardware resources for this application; the system requires less than 200 MB of RAM, which accounts for just 4.88 % of the total 4 GB on-board RAM. Therefore, RPi4 offers a portable solution that consumes less energy and costs less than a PC, without sacrificing accuracy or reliability.

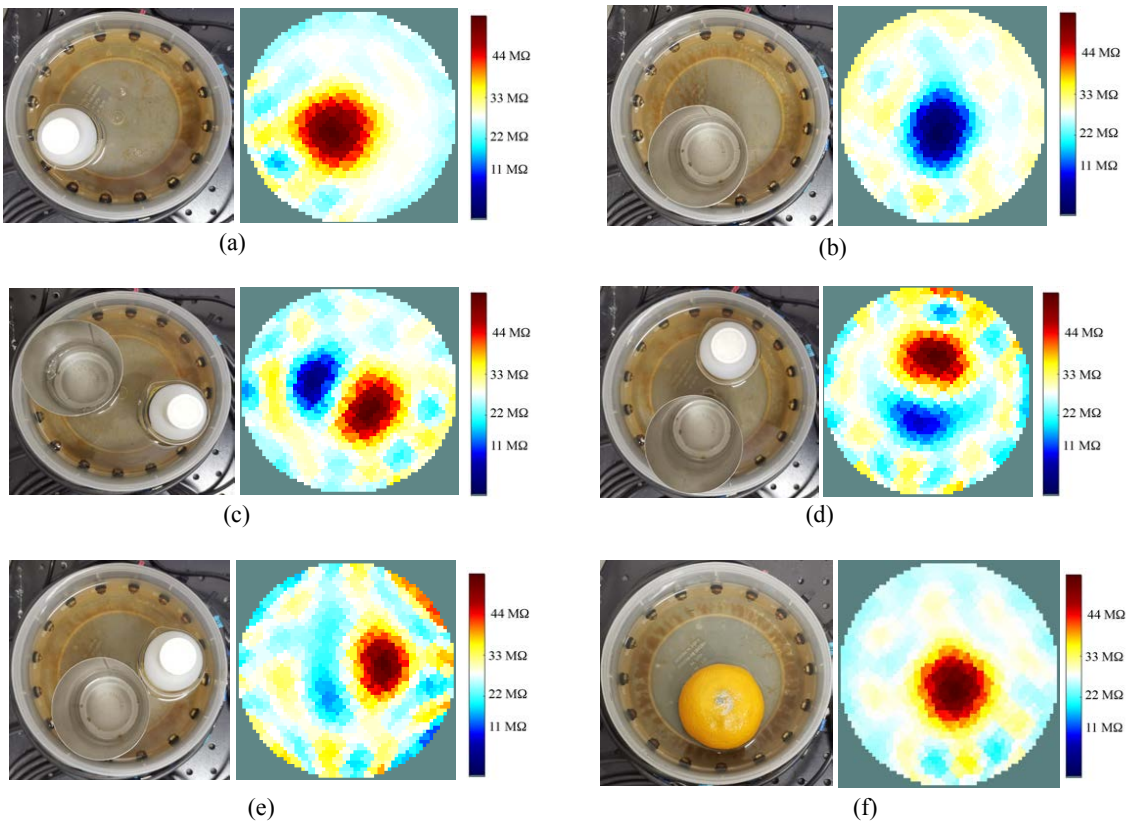

Figure 32: Real-time image reconstruction on RPi4: (a) Glass object under test, (b) Metal object under test, (c) Metal and glass object under test, (d) Metal and glass in different positions, (e) Metal and glass in different positions, (f) An orange under test.

4.4. Performance comparison between PC and RPi4

This section is presented for the purpose of comparing the performance of the proposed EIT system on different kind of hardware. Table 3 compares the features of our proposed EIT system on RPi4 and on the PC. The PC has the following features: Laptop Dell Inc. Inspiron 7559 x64 bit, processor Intel(R) Core (TM) i5-6300HQ, CPU with 2.30 GHz clock, 2301 MHz Quad Core, 16 GB of DDR SDRAM 3L at 1600 MHz, and Microsoft Windows 10 Pro version 10.0.18362 as the operating system. On the other hand, the RPi4 used has the following features: Raspberry Pi 4, 4 GB RAM, Model B with clock working at 1.5 GHz, and a 64-bit Quad Core ARMv8 CPU. In terms of hardware, the PC clock is 65.21 % faster than RPi4, and the PC has 16 GB of RAM memory, while RPi4 only has 4 GB. In terms of software, the PC has the operating system Windows 10 Pro and Matlab R2016b, while RPi4 uses Raspbian 4.19 as the operating system, which is a free distribution of GNU/Linux, and GNU Octave 4.4.1 is used as the programming language, under free license. The same EIDORS library and the same firmware developed in this article were used in both types of hardware. Finally, another important factor is the total cost of the EIT system developed. The cost of the PC-based system is $1000.00 U.S. dollars while RPi4 costs only $250.00 U.S. dollars. The PC is therefore four times more expensive than RPi4 (Note: These estimations are an average. Also, the Matlab license can be disregarded when running Octave on PC). Thus, one of the aims of this paper is to present the development of a portable, reliable and low-cost EIT system without losing any information or quality in the image-forming process. There are some trade-offs to be consider, as mentioned above and as shown in Table 3, the price of the PC is higher but also the image reconstruction on PC is faster, while in RPi4 is slower, however, RPi4 is lighter and smaller, this allows us for example easy transport. For example, some of the applications in geology, require to go to places where there is no electricity, then a smaller battery will be able to make the proposed EIT system to work in potential EIT applied in soil study. On the other hand, a PC is easier to use, however, RPi4 has already a lot of information available on internet of how to use it. Most people have portable PCs, nevertheless, if the EIT system is used with a PC it will require the user to take his PC dedicated to this task, while if having a portable option, the user may leave the EIT system working separated from his PC, e.g. a PC may play a movie, but some dedicated devices like a Smart TV do the same, without the need of a PC. Many other trade-offs can

be consider as in every system that can be used in a PC or dedicated device, in the end, the user will define whether if he will prefer to use the EIT system with a PC or with RPI4.

Table 3: Comparison of characteristics of the proposed EIT on the PC versus RPi4.

Features	Proposed EIT system on PC	Proposed EIT system on RPi4
Central Processing Unit (CPU)	Intel (R) Core (TM) i5-6300HQ	ARMv8
Architecture	Quad Core, x86-64 bit	Quad Core, ARM 64 bit
Clock	2.30 GHz	1.50 GHz
Random-access memory (RAM)	16 GB DDR-SDRAM	4 GB DDR4
Operating system	Windows 10 Pro 10.0.18362	Raspbian 4.19
Software	Matlab R2016b	GNU Octave 4.4.1
Power consumption	350-400W	5-15W
Communication	USB	USB
Networking	WiFi, Ethernet, Bluetooth	WiFi, Ethernet, Bluetooth
Internet connectivity	Yes	Yes
Weight	7.2 kg	4.5 kg
Dimensions (average)	300x200x40 [mm]	82x56x19.5 [mm]
Data acquisition hardware [U.S. Dollars]	$100.00	$100.00
Software license cost [U.S. Dollars]	Matlab single user $150.00	Free
Total cost [U.S. Dollars]	$1,000.00	$250.00

Table 4 shows a comparison between the execution times of the software running on a PC and on RPi4. It can be observed that the results on the PC are executed more quickly across the four processes required to perform the EIT. Furthermore, when the proposed EIT system uses a 4 kHz signal, the average RPi4/PC ratio is 4.35, while with a 40 kHz signal, the average ratio is 5.03; however, the total cost of the PC-based system is 400 % higher than the RPi4.

Table 4: Comparison between the execution times of the algorithms on a PC vs. RPi4

Process	Algorithm	4 kHz test on PC [s]	4 kHz test on RPI4 [s]	Avg. Ratio RPi4/PC	40 kHz test on PC [s]	40 kHz test on RPI4 [s]	Avg. Ratio RPi4/PC
1	Load RAW data	4.177604	11.2553	2.6942	3.091808	8.09153	2.617087
2	Averaging algorithm B	0.218396	10.7864	49.38918	0.203601	10.7508	52.80328
3	Averaging algorithm p1	0.222845	10.7729	48.34257	0.201479	10.7654	53.43187
4	Averaging algorithm p2	0.220746	10.7498	48.6976	0.202687	10.7556	53.06507
5	Averaging algorithm p3	0.218783	10.7878	49.30822	0.213301	10.7607	50.44843
6	Averaging algorithm p4	0.37518	10.7401	28.62653	0.219097	10.7455	49.04449
7	Averaging algorithm p5	0.322562	10.7741	33.40164			
8	Averaging algorithm p6	0.229163	10.7615	46.96002			
9	Comparison algorithm 1	0.001892	0.010285	5.435994	0.001496	0.011233	7.508623
10	Comparison algorithm 2	0.000868	0.010255	11.81463	0.000516	0.007937	15.38169
11	Comparison algorithm 3	0.000726	0.010808	14.88733	0.000534	0.008557	16.02449
12	Comparison algorithm 4	0.000642	0.010731	16.71495			
13	Comparison algorithm 5	0.000458	0.01052	22.96943			
14	Comparison algorithm 6	0.000367	0.010801	29.43079			
15	Generate image 1	1.679503	7.19625	4.28475	1.523613	8.41856	5.525393
16	Generate image 2	1.752863	5.43297	3.099484	1.547319	5.43366	3.511661
17	Generate image 3	1.548002	5.46065	3.527547	1.569827	5.51226	3.511381
18	Generate image 4	1.654057	5.51766	3.335834	1.57206	5.39322	3.430671
19	Generate image 5	2.312579	5.39704	2.333775			
20	Generate image 6	2.119322	5.46788	2.580014			
21	Generate image 1	2.270907	7.23758	3.187088	1.651131	8.92157	5.403308
22	Generate image 2	1.732666	5.51461	3.182731	1.599166	5.52643	3.45582
23	Generate image 3	1.641541	5.44866	3.319235	1.604967	5.44634	3.393428
24	Generate image 4	3.048024	5.45532	1.789789	1.629613	5.43712	3.336449
25	Generate image 5	1.841157	5.47907	2.975884			
26	Generate image 6	2.059301	5.47139	2.656916			
27	Generate image 1	2.069203	7.10464	3.433516	1.62543	7.24641	4.45815
28	Generate image 2	1.997686	5.35105	2.678624	1.715603	5.57153	3.247564
29	Generate image 3	1.810128	5.43402	3.002009	1.656268	5.46319	3.298494
30	Generate image 4	1.822647	5.45504	2.992922	1.601753	5.45979	3.408634
31	Generate image 5	2.371916	5.4942	2.316355			
32	Generate image 6	1.663407	5.76794	3.467546			
33	Generate image 1	2.22097	7.48894	3.371923	1.624438	7.578	4.664998
34	Generate image 2	1.872019	5.3701	2.868614	1.82086	5.3885	2.959316
35	Generate image 3	1.726198	5.47857	3.173778	1.655939	5.39759	3.259534
36	Generate image 4	2.378732	5.42829	2.28201	1.681663	5.4113	3.217827
37	Generate image 5	2.231945	5.48047	2.455468			
38	Generate image 6	2.68666	5.56951	2.073024			
39	Generate image 1	1.740418	7.57327	4.351409	1.692744	7.34871	4.3413
40	Generate image 2	1.57499	5.36714	3.40773	1.703104	5.41973	3.182266
41	Generate image 3	1.755426	5.39082	3.070947	1.705708	5.51775	3.234874
42	Generate image 4	1.573828	5.44001	3.456547	1.712771	5.44383	3.178376
43	Generate image 5	1.58774	5.4896	3.457493			
44	Generate image 6	1.884791	5.44492	2.888872			
	TOTAL	58.62863	173.2076	2.954318	32.89398	121.3355	3.688684

4.5. Comparison versus related work

Related work of EIT has been studied and compared to our proposed EIT system. Table 5 shows a compendium of features from several revised articles. In Deng et al. (2018), the authors report an EIT system with an 12 bit ADC that has 2400 kSPS, for data acquisition they use the MCU STM32F446RE and do not mention the software for image reconstruction used. In Ansory et al. (2018), the authors use a 16 bit ADC with 0.860 kSPS, which is the

lowest sample rate, for data acquisition they use the MCU Arduino UNO, and they perform the image reconstruction by using EIDORS running on a PC. In Widodo Aris (2018), the authors use a 16 bit ADC with 0.860 kSPS, for data acquisition they also use the MCU Arduino UNO and a Raspberry Pi 3 as CPU, the main difference of this related work, is that they use a different software for image reconstruction, i.e., they use the Gauss-Newton for Python. In Sohal et al. (2014), the authors use a 12 bit ADC with 65000 kSPS, which is the highest sample rate, for data acquisition they use an FPGA and DSP, and for image reconstruction they use a PC running the GREIT algorithm. In Kusche et al. (2015), the authors use a 14 bit ADC with 25000 kSPS, for data acquisition they use an FPGA, and the image reconstruction is made on a PC running EIDORS, NETGEN and GREIT algorithm. Finally, as can be seen in the table 5, the related work do not report details of the designed circuits, nor of the algorithms implemented on single board computers. On the other side, it is also important to note that when one have an ADC with higher sample rate and higher communication speed between the DAQ device and the CPU, one can get more images per minute (frames per minute).

Table 5: Comparison of proposed EIT system versus other related work.

Feature	Proposed system	Ref. Deng et al. (2018)	Ref. Ansory et al. (2018)	Ref. Widodo Aris (2018)	Ref. Sohal et al. (2014)	Ref. Kusche et al. (2015)
ADC resolution [bit]	24	12	16	16	12	14
Sample rate [kSPS]	30	2400	0.860	0.860	65000	25000
Device for data acquisition	Arduino MEGA	STM32F446RE	Arduino UNO	Arduino UNO	FPGA & DSP	FPGA
Communication Speed [kbps]	500	921.6	N/A	N/A	N/A	40000
Multiplexer	ADG1406	ADG726	ADG731BSUZ	AD506AKNZ	N/A	N/A
CPU	Raspberry Pi4	PC	PC	Raspberry Pi3	PC	PC
Electronic diagram shown	Yes	No	No	No	No	No
Embedded Algorithms Shown	Yes	No	No	No	No	No
Software for Image reconstruction	EIDORS	N/A	EIDORS	Gauss-Newton for Python	GREIT algorithm	EIDORS, NETGEN and GREIT algorithm

4.6. Pictures of the EIT device working on PC using Matlab and on RPI4 Using GNU Octave

The following figures show examples of the device working, in each photo there is a screen monitor where the image formed is shown, at the same time the vessel can be seen with the object of study inside of it, Figure 33 depicts the device connected to a PC by using Matlab to make the image reconstruction, and Figure 34 shows the device connected to the SBC RPi4, it can be observed in the monitor screen the well-known Matlab interface, and the well-known Raspian interface. This tests have an upgrade in speed, the data transfer speed used for this tests was 1000000 bauds, which did not work in the first stages of the experiment, due to a lack of synchronization, by upgrading and adjusting the programmed software this was now possible, and the data transfer speed of the EIT system was upgraded to 4 times its original speed.

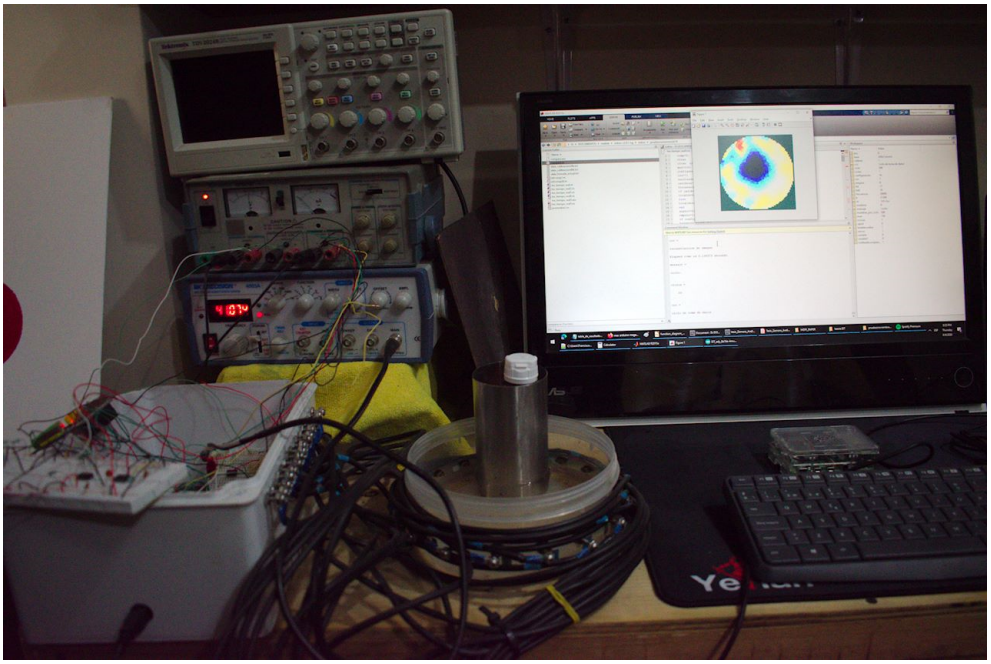

Figure 33: Picture of the proposed EIT system using a PC.

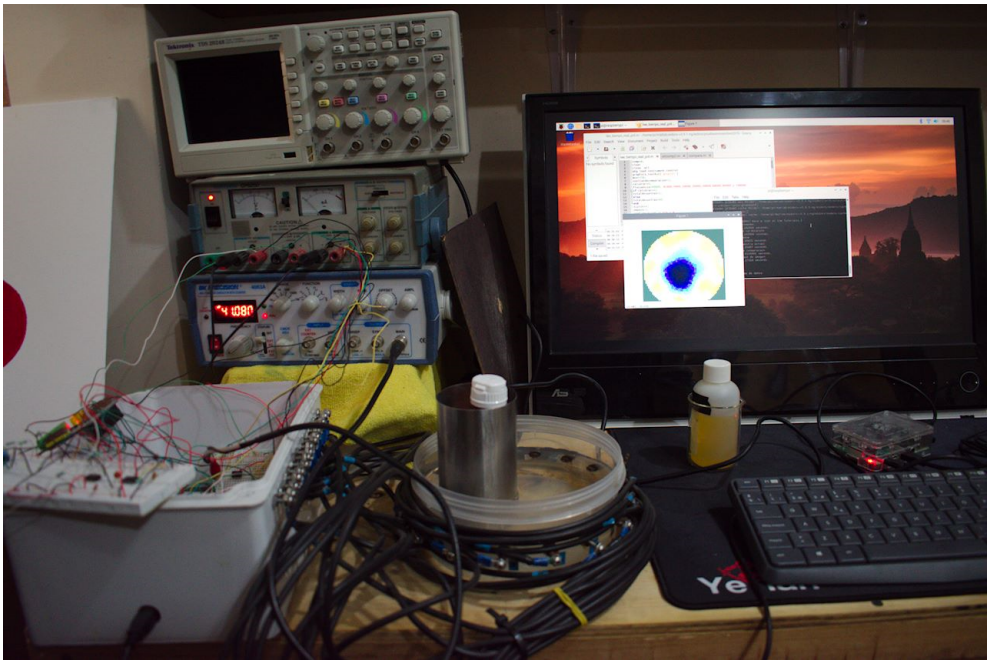

Figure 34: Picture of the proposed EIT system using RPi4.

Chapter V

5. Conclusions

The proposed EIT system showed satisfactory results since the multiple tests performed to verify functionality were very successful. Nonetheless, some stages can be improved to enhance performance, such as ADC sample rate and communication between DAQ device and CPU: the faster the ADC and communication, the sooner a complete cycle can be performed. Special circuits could also be used to reduce noise in the measurements. From the experiments with the PC and RPi4, it can be concluded that the numerical computation and reconstructed images deliver practically the same results, because both types of hardware perform numerical calculations according to the IEEE 754 standard for floating-point operations. Besides the ADC hardware, a software adjustment is necessary to perform statistics on the measurements, as shown in the Algorithm 1 by using 250 samples, a statistical mean was calculated in the last 120 samples to determine the best measured value with the ADC. Another important aspect in the proposed EIT system is the method used to read impedance; in this paper, the adjacent method was used, but other configurations can also be used to read impedance. The algorithms and hardware can be replicated and are open to improvements, for example by using a faster ADC or a DDS signal generator. The main purpose of this research was to develop an EIT system as a whole, which would enable real-time image reconstruction by using an RPi4. By processing the same raw data obtained from the impedance acquisition stage in both PC and RPi4 hardware, it was showed that ARM architecture can perform the same process with practically the same quantitative results, sacrificing only processing time, while consuming much less power and fewer hardware resources, with open software, fast development and low-cost hardware, just as shown in the cost-benefit analysis in Tables 3-4. The use of RPi4 provides the EIT system with portability, offering potential industrial and medical applications. Finally, the proposed system proves that a portable and reliable application on an SBC is possible and offers an excellent cost-benefit ratio in comparison with a PC, considering precision, accuracy, resolution, energy consumption, price, size, weight, portability and reliability.

5.1. Future Work

The future work will upgrade the proposed EIT system, the next is a list of possible improvements, that can be made to this EIT system.

- Upgrading the ADC: The analog to digital converter is a key piece that affects directly in the time required to generate a complete cycle of measurements, as mentioned, in this work, as minimum, 6 seconds were necessary to wait for a complete cycle measurement, the ADC1256 has a 30KSPS (sampling frecuency) this means that if only the sampling frequency is 10 times higher, a complete measurement cycle will now need only 600ms to be performed, therefore changing the ADC to one with a better sample rate is a good upgrade idea.

- Adding demodulation: Instead of using a peak-detector, there are some models that uses a demodulator to obtain a better impedance value, because demoduling an AC signal can gives us information not only of the Real value of the impedance, but a complete complex value of the impedance measured. The demodulator nowadays is applied digitally, this means that an even faster ADC should be used, most of the frequencies used in EIT are between 10 to 100kHz, therefore at least a 1GSPS ADC will be necessary to apply a digital demodulator, improving its accuracy while measuring voltage and its speed of completing measurement cycles.

- Paralleling the software: A software upgrade that can be applied and will be very useful, is the use of parallel algorithms, this means that while a single processor can do all the programmed tasks, now, several processors may receive different tasks, data, or instructions to be executed, this will improve the system efficiency and effectiveness, taking advantage of the multi-cores of the SBC RPI4.

- Upgrading the SBC: As mentioned in this work, the SBC RPI4 requires about to 4 to 6 seconds to perform the image reconstruction algorithm, therefore an update changing the SBC would be a good choice, one of the proposed SBC that can be applied is the nVidia Jetson nano that has faster cores and also multiGPU cores.

- Using Machine Learning and Deep Learning for pattern recognition: Recently it has been verified and demonstrated that the methods based on machine learning and deep learning are

very precise and exact for the recognition of patterns in images, which would be interesting to use these techniques in EIT images.

- The proposed EIT system can be prepared to be used in the area of Earth Sciences, particularly to characterize different layers of the earth's surface.

-Development of reconstruction algorithms focused in obtaining a better spatial precision and less noise.

-Finally, the proposed EIT system could be used in the health sector for patients with suspected of COVID-19, this by means of a research work to characterize the impedance of lungs as positive and negative diagnosis cases, so this this could be a low-cost and fast development alternative solution for early diagnosis of COVID-19.

Appendix

6. Printed Circuit Boar design

Figure 36, 35 and 37 shows the designed Circuit, Printed circuit board (PCB) and gerber file for the proposed EIT system, the PCB contains the circuitry of all 4 multiplexers, the high-precision peak detector and the designed constant current driver, it has connectors to be attached to the MCU, to the 16 electrodes and to an external AC voltage source, also it can be connected directly to another AC constant current source, by not using the designed one.

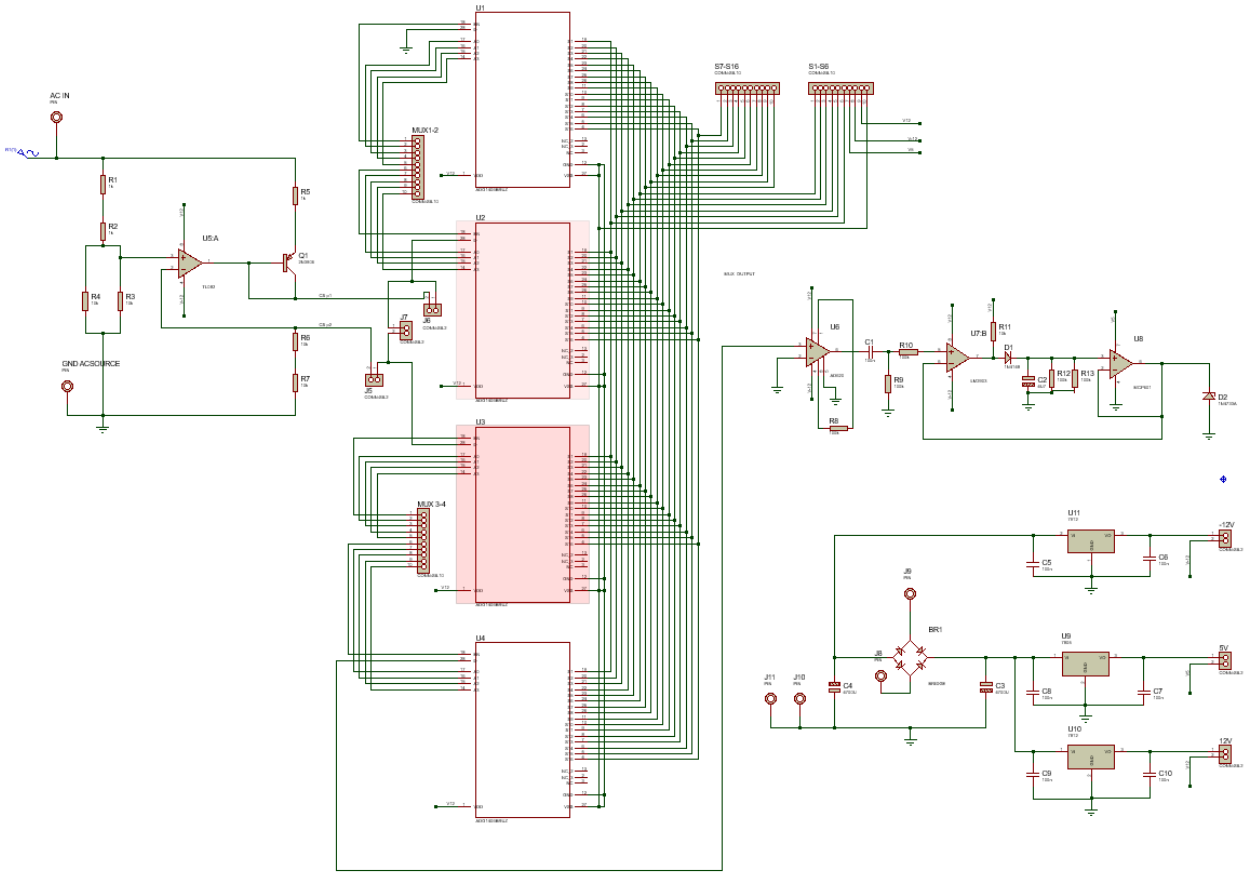

Figure 35: Circuit designed for the proposed EIT system.

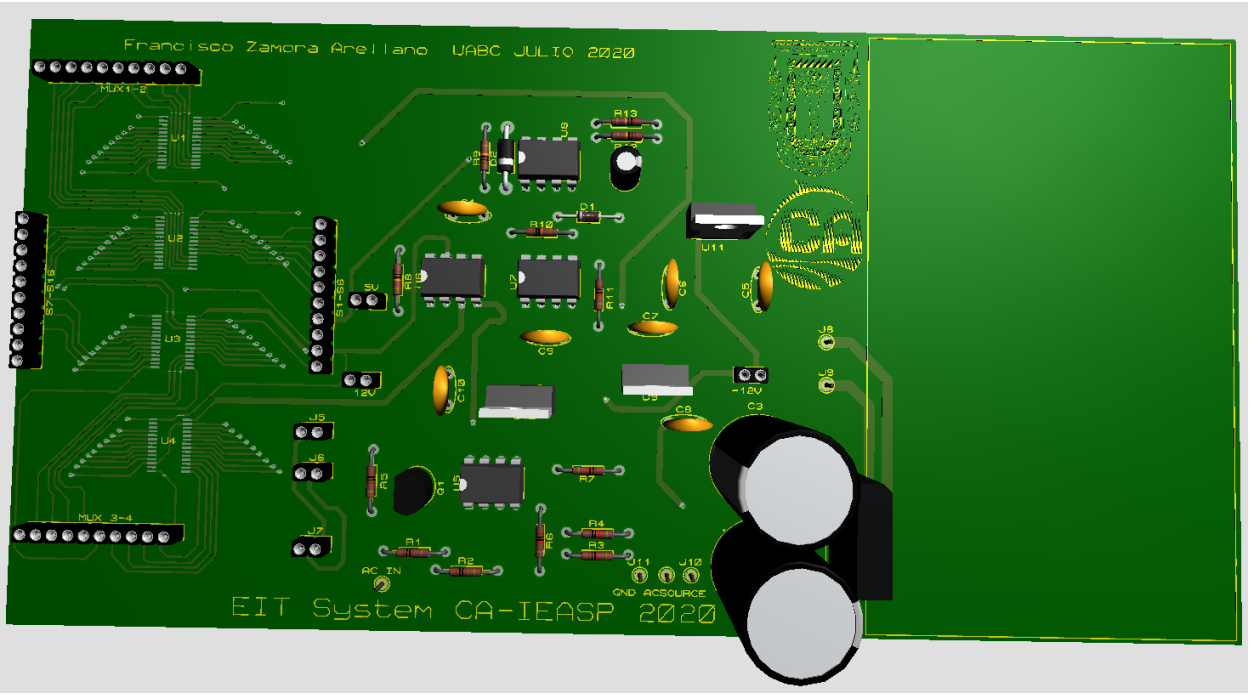

Figure 36: PCB designed for the proposed EIT system.

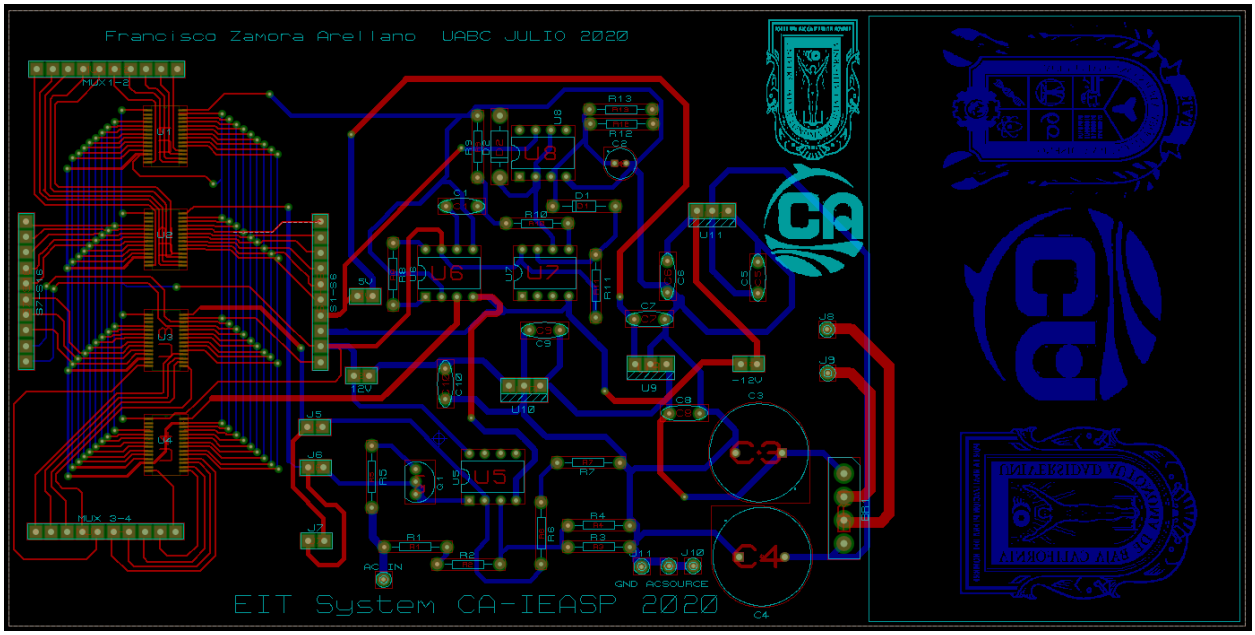

Figure 37: Gerber designed for the proposed EIT system.

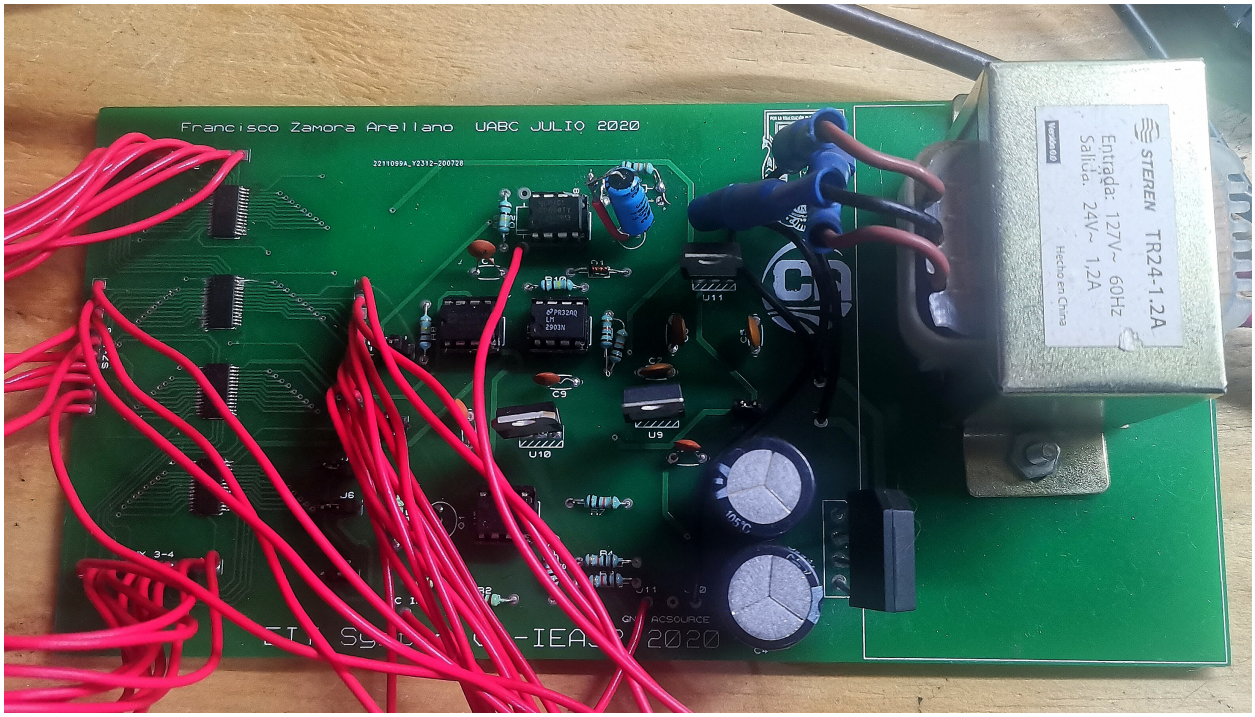

Figure 38: Printed circuit board with components of EIT system.

Referencias

A. Adler and W. R. Lionheart. Uses and abuses of EIDORS: An extensible software base for EIT. *Physiol. Meas.*, 27(5):S25–42, 2006. doi: 10.1088/0967-3334/27/5/S03.

O. Aguirre-Castro, E. Inzunza-González, E. García-Guerrero, E. Tlelo-Cuautle, O. López-Bonilla, J. Olguín-Tiznado, and J. Cárdenas-Valdez. Design and Construction of an ROV for Underwater Exploration. *Sensors*, 19(24):5387, 2019. doi: 10.3390/s19245387.

K. Ain, D. Kurniadi, S. Suprijanto, and O. Santoso. Dual modality electrical impedance and ultrasound reflection tomography to improve image quality. *Journal of Electrical Bioimpedance*, 8(1):3–10, 2017. doi: 10.5617/jeb.3852. URL `https://content.sciendo.com/view/journals/joeb/8/1/article-p3.xml`.

S. Akhavan and S. Hashemian. The role of electrical impedance tomography for monitoring during bronchoscopy: A case report. *J Crit Care*, 48:311–313, 2018. doi: 10.1016/j.jcrc.2018.09.028.

K. Alessio, B. Tischer, M. Voss, I. Teixeira, B. Brendler, F. Duarte, G. Helfer, A. Costa, and J. Barin. Open source, low-cost device for thermometric titration with non-contact temperature measurement. *Talanta*, 216, 2020. doi: 10.1016/j.talanta.2020.120975.

J. Anso, T. W. Balmer, Y. Jegge, H. Kalvoy, B. J. Bell, C. Dur, E. M. Calvo, T. M. Williamson, N. Gerber, D. Ferrario, F. Forterre, P. Buchler, A. Stahel, M. Caversaccio, S. Weber, and G. K. Electrical Impedance to Assess Facial Nerve Proximity During Robotic Cochlear Implantation. *IEEE Trans Biomed Eng*, 66(1):237–245, 2019. doi: 10.1109/TBME.2018.2830303.

A. Ansory, P. Prajitno, and S. K. Wijaya. Design and development of electrical impedance tomography system with 32 electrodes and microcontroller. In D. Radon, W. Yudan, R. Ghiska, and Wulan, editors, *2nd Biomedical Engineering Recent Progress in Biomaterials, Drugs Development, and Medical Devices*, number AIP Conf. Proc. 1933, 040023-1–040023-5, 2018. doi: 10.1063/1.5023993.

K. Y. Aristovich, B. C. Packham, H. Koo, G. S. dos Santos, A. McEvoy, and D. S. Holder. Imaging fast electrical activity in the brain with electrical impedance tomography. *Neuro-*

Image, 124:204–213, 2016. ISSN 1053-8119. doi: 10.1016/j.neuroimage.2015.08.071. URL http://www.sciencedirect.com/science/article/pii/S1053811915007922.

J. Avery, T. Dowrick, M. Faulkner, N. Goren, and D. Holder. A Versatile and Reproducible Multi-Frequency Electrical Impedance Tomography System. *Sensors (Basel)*, 17(2):280, 2017. doi: 10.3390/s17020280.

A. Aydi, A. Mhimdi, I. Hamdi, S. Touaylia, and A. Sdiri. Application of electrical resistivity tomography and hydro-chemical analysis for an integrated environmental assessment. *Environmental Nanotechnology, Monitoring and Management 14 (2020)*, 2020. doi: 10.1016/j.enmm.2020.100351.

J. Badr, Y. Fargier, S. Palma-Lopes, F. Deby, B. Jean-Paul, S. Delepine-Lesoille, L.-M. Cottineau, and V. Geraldine. Design and validation of a multi-electrode embedded sensor to monitor resistivity profiles over depth in concrete. *Construction and Building Materials 223 (2019)*, 2019. doi: 10.1016/j.conbuildmat.2019.06.226.

T. K. Bera. Applications of Electrical Impedance Tomography(EIT): A Short Review. *IOP Conference Series: Materials Science and Engineering*, 331:012004, 2018. doi: 10.1088/1757-899x/331/1/012004.

R. A. Borsoi, J. C. C. Aya, G. H. Costa, and J. C. M. Bermudez. Super-resolution reconstruction of electrical impedance tomography images. *Computers & Electrical Engineering*, 69:1–13, 2018. ISSN 00457906. doi: 10.1016/j.compeleceng.2018.05.013.

C. Dimas, N. Uzunoglu, P. P. Sotiriadis. Electrical Impedance Tomography Image Reconstruction: Impact of Hardware Noise and Errors. *Proceedings of 2019 8th International Conference on Modern Circuits and Systems Technologies (MOCAST), Thessaloniki, Greece*, pages 13–15, 2019. doi: 10.1109/MOCAST.2019.8741913.

J. Cagan and J. Rosler. Design of multiplexer for electrical impedance tomography. *Materials Today: Proceedings*, 4(5):5755–5760, 2017. doi: 10.1016/j.matpr.2017.06.041.

M. Calvo Hernando. Electronic Instrumentation for a 3D Electrical Impedance Tomography Application. *Master of Science Thesis, Tampere University*, 2018.

P. Caro, A. García, and J. M. Reyes. Stability of the Calderón problem for less regular conductivities. *Journal of Differential Equations*, pages 469–492, 2013. doi: https://doi.org/10.1016/j.jde.2012.08.018.

C. Das, S. Chakraborty, A. Karmakar, and S. Chattopadhyay. On-chip detection and quantification of soap as an adulterant in milk employing electrical impedance spectroscopy. pages 1–4, 2018. doi: 10.1109/ISDCS.2018.8379634.

Q. Deng, Y. Su, S. Hu, X. Xiong, R. Juan, Y. Zhang, and H. Ma. A Parallel Impedance Measurement System for Electrical Impedance Tomography System with Multi-Microcontroller-Unit Architecture. *2018 IEEE International Conference on Manipulation, Manufacturing and Measurement on the Nanoscale (3M-NANO) 13-17 August, Hangzhou*, 2018. doi: 10.1109/3M-NANO.2018.8552230.

C. Dimas, N. Uzunoglu, and P. P. Sotiriadis. A Parametric EIT System Spice Simulation with Phantom Equivalent Circuits. *Technologies*, 8(1):13, 2020. doi: 10.3390/technologies8010013.

E. Dunne, A. Santorelli, B. McGinley, G. Leader, M. O'Halloran, and E. Porter. Image-based classification of bladder state using electrical impedance tomography. *Physiol. Meas.*, 39 (12):124001, 2018. doi: 10.1088/1361-6579/aae6ed.

A. Dupré and S. Mylvaganam. A Simultaneous and Continuous Excitation Method for High-Speed Electrical Impedance Tomography with Reduced Transients and Noise Sensitivity. *Sensors*, 18(4):1013, 2018. doi: 10.3390/s18041013.

M. Faulkner, S. Hannan, K. Aristovich, J. Avery, and D. Holder. Feasibility of imaging evoked activity throughout the rat brain using electrical impedance tomography. *Neuroimage*, 178: 1–10, 2018. doi: 10.1016/j.neuroimage.2018.05.022.

X. Fernández-Fuentes, D. Mera, A. Gómez, and I. Vidal-Franco. Towards a Fast and Accurate EIT Inverse Problem Solver: A Machine Learning Approach. *Electronics*, 7(12), 2018. doi: 10.3390/electronics7120422.

I. Frerichs, J. Hinz, P. Herrmann, G. Weisser, G. Hahn, T. Dudykevych, M. Quintel, and G. Hellige. Detection of local lung air content by electrical impedance tomography com-

pared with electron beam ct. *Journal of Applied Physiology*, 93(2):660–666, 2002. doi: 10.1152/japplphysiol.00081.2002. PMID: 12133877.

P. O. Gaggero, A. Adler, J. Brunner, and P. Seitz. Electrical impedance tomography system based on active electrodes. *Physiol Meas*, 33(5):831–47, 2012. doi: 10.1088/0967-3334/33/5/831.

X. Gao, T. Wei, H. Dong, and Y. Song. Damage detection in 2.5D C/SiC composites using electrical resistance tomography. *Journal of the European Ceramic Society 39 (2019)*, 2019. doi: 10.1016/j.jeurceramsoc.2019.04.046.

Z. R. Gatabi, R. Mohammadpour, J. R. Gatabi, M. Mirhoseini, M. Ahmadi, and P. Sasanpour. Sandblasting improves the performance of electrodes of miniature electrical impedance tomography via double layer capacitance. *Heliyon*, 6(4):e03652, 2020. doi: 10.1016/j.heliyon.2020.e03652.

A. Gautam, A. Kumar, K. Kinjalk, J. Thangaraj, and V. Priye. A Low Cost FBG Based Online Weight Monitoring System. *IEEE Sensors Journal*, 20(8):4207–4214, 2020. doi: 10.1109/JSEN.2019.2961688.

D. Gisser, D. Isaacson, and N. J.C. Current topics in impedance imaging. *Clinical Physics and Physiological Measurement*, 8(4A):39–46, 1987. doi: 10.1088/0143-0815/8/4a/005.

C.-H. Gow, M.-Y. Chang, Z. Zhao, and K. Moller. Patient-ventilator asynchrony identified with electrical impedance tomography. *IFAC-PapersOnLine*, 51(27):52–55, 2018. doi: 10.1016/j.ifacol.2018.11.607.

M. Gutierrez-Lopez, J. Prado-Olivarez, J. Diaz-Carmona, C. A. Herrera-Ramírez, J. A. Gutierrez-Gnecchi, and C. G. Medina-Sánchez. Electrical Impedance-Based Methodology for Locating Carcinoma Emulators on Breast Models. *Journal of Sensors*, 2019:1–16, 2019. ISSN 1687-725X 1687-7268. doi: 10.1155/2019/8587191.

S. Hannan, M. Faulkner, K. Aristovich, J. Avery, M. C. Walker, and D. S. Holder. In vivo imaging of deep neural activity from the cortical surface during hippocampal epileptiform events in the rat brain using electrical impedance tomography. *Neuroimage*, 209:116525, 2020. doi: 10.1016/j.neuroimage.2020.116525.

R. Harikumar, R. Prabu, and S. Raghavan. Electrical Impedance Tomography (EIT) and Its Medical Applications: A Review. *International Journal of Soft Computing and Engineering (IJSCE)*, 3:2231–2307, 2013. doi: D1821093413/2013BEIESP.

J. Hu and M. Soleimani. Combining Multiple Boundary Shapes in Deformable EIT a Potential Use in Breast Imaging. *IEEE Sensors Letters*, 4(4):1–4, 2020. doi: 10.1109/LSENS.2020.2978289.

J.-J. Huang, Y.-H. Hung, J.-J. Wang, and B.-S. Lin. Design of wearable and wireless electrical impedance tomography system. *Measurement*, 78:9–17, 2016. doi: 10.1016/j.measurement.2015.09.031.

P. Ibba, A. Falco, A. Rivadeneyra, and P. Lugli. Low-cost bio-impedance analysis system for the evaluation of fruit ripeness. pages 1–4, 2018. doi: 10.1109/ICSENS.2018.8589541.

J. Karsten, K. MBohlmann, B. Sedemund-Adib, J. Wnent, H. Paarmann, P. Iblher, T. Meier, and H. Heinze. Electrical impedance tomography may optimize ventilation in a postpartum woman with respiratory failure. *International Journal of Obstetric Anesthesia*, 22(1):67–71, 2013. doi: 10.1016/j.ijoa.2012.09.002.

R. Kusche, A. Malhotra, M. Ryschka, G. Ardelt, P. Klimach, and S. Kaufmann. A FPGA-Based Broadband EIT System for Complex Bioimpedance Measurements—Design and Performance Estimation. *Electronics*, 4(3):507–525, 2015. ISSN 2079-9292. doi: 10.3390/electronics4030507.

D. Liu, D. Smyl, and J. Du. A Parametric Level Set-Based Approach to Difference Imaging in Electrical Impedance Tomography. *IEEE Trans Med Imaging*, 38(1):145–155, 2019. doi: 10.1109/TMI.2018.2857839.

S. Liu, J. Jia, Y. D. Zhang, and Y. Yang. Image reconstruction in electrical impedance tomography based on structure-aware sparse bayesian learning. *IEEE Transactions on Medical Imaging*, 37(9):2090–2102, 2018. doi: 10.1109/TMI.2018.2816739.

S. Liu, Y. Huang, H. Wu, C. Tan, and J. Jia. Efficient multitask structure-aware sparse bayesian learning for frequency-difference electrical impedance tomography. *IEEE Transactions on Industrial Informatics*, 17(1):463–472, 2021. doi: 10.1109/TII.2020.2965202.

H. Ma, H. Li, X. Liu, W. Li, J. Xia, B. Liu, X. Shi, X. Dong, and F. Fu. Real-Time Monitoring of Contact Impedance From Multiple Electrode–Scalp Interfaces During Cerebral Electrical Impedance Tomography. *IEEE Access*, 7:95186–95196, 2019. doi: 10.1109/access.2019.2928580.

S. Makarov, M. Horner, and G. Noetscher, editors. *Brain and Human Body Modeling: Computational Human Modeling at EMBC 2018*. Cham (CH) Springer, 2019. doi: 10.1007/978-3-030-21293-3.

E. Malone, G. Sato dos Santos, and D. Holder. A Reconstruction-Classification Method for Multifrequency Electrical Impedance Tomography. *IEEE Transactions on Medical Imaging*, 34(7):1486–1497, 2015. doi: 10.1109/TMI.2015.2402661.

N. V. Mane and R. P. Mudhalwadkar. Banana ripeness assessment by impedance spectroscopy. pages 527–529, 2017. doi: 10.1109/ICPCSI.2017.8392349.

H. Mao, X. Yi, H. Mao, W. Tang, Z. Huang, X. Li, and L. Sun. Fatigue damage detection and location of metal materials by electrical impedance tomography. *Results in Physics*, 15, 2019. doi: 10.1016/j.rinp.2019.102664.

M. Molinari. High fidelity imaging in electrical impedance tomography. *Department of electronics and computer science, University of Southampton*, 1(1):142, 2003. doi: https://eprints.soton.ac.uk/45805/.

M. Nirmala and K. Malarvizhi. Internet of things based solar powered truck. *Test Engineering and Management*, 83:9358–9365, 2020.

C. Nykvist, M. Larsson, A. Sodhro, and A. Gurtov. A lightweight portable intrusion detection communication system for auditing applications. *International Journal of Communication Systems*, 33(7), 2020. doi: 10.1002/dac.4327.

D. D. Pak, N. I. Rozhkova, M. N. Kireeva, M. V. Ermoshchenkova, A. A. Nazarov, D. K. Fomin, and N. A. Rubtsova. Diagnosis of Breast Cancer Using Electrical Impedance Tomography. *Biomedical Engineering*, 46(4):154–157, 2012. doi: 10.1007/s10527-012-9292-7. URL `https://doi.org/10.1007/s10527-012-9292-7`.

G. Perchiazzi and H. Wrigge. Acute Respiratory Distress Syndrome (ARDS): Pathophysiological Insights and Lung Imaging. *J Clin Med*, 8(12), 2019. doi: 10.3390/jcm8122171.

J. Priou, Y. Lecieux, M. Chevreuil, V. Gaillard, C. Lupi, D. Leduc, E. Roziere, R. Guyard, and F. Schoefs. In situ DC electrical resistivity mapping performed in a reinforced concrete wharf using embedded sensors. *Construction and Building Materials 211 (2019)*, 2019. doi: 10.1016/j.conbuildmat.2019.03.152.

C. Putensen, B. Hentze, S. Muenster, and T. Muders. Electrical Impedance Tomography for Cardio-Pulmonary Monitoring. *J Clin Med*, 8(8), 2019. doi: 10.3390/jcm8081176.

J. Radon. On the determination of functions from their integral values along certain manifolds, Translated bye P.C. Parks (1986). *IEEE Transactions on Medical Imaging*, MI-5(4): 170–176, 1917. doi: 10.1109/TMI.2015.2402661.

P. Rai, S. Oh, P. Shyamkumar, M. Ramasamy, R. E. Harbaugh, and V. K. Varadan. Nano-Bio- Textile Sensors with Mobile Wireless Platform for Wearable Health Monitoring of Neurological and Cardiovascular Disorders. *Journal of The Electrochemical Society*, 161 (2):B3116–B3150, 2013. doi: 10.1149/2.012402jes.

M. Rapin, F. Braun, A. Adler, J. Wacker, I. Frerichs, B. Vogt, and O. Chetelat. Wearable Sensors for Frequency-Multiplexed EIT and Multilead ECG Data Acquisition. *IEEE Transactions on Biomedical Engineering*, 66(3):810–820, 2019. doi: 10.1109/TBME.2018.2857199.

S. Russo, S. Nefti-Meziani, N. Carbonaro, and A. Tognetti. A Quantitative Evaluation of Drive Pattern Selection for Optimizing EIT-Based Stretchable Sensors. *Sensors*, 17(9): 1999, 2017a. doi: 10.3390/s17091999.

S. Russo, S. Nefti-Meziani, N. Carbonaro, and A. Tognetti. Development of a High-Speed Current Injection and Voltage Measurement System for Electrical Impedance Tomography-Based Stretchable Sensors. *Technologies*, 5(3):48, 2017b. doi: 10.3390/technologies5030048.

E. Ryndin, B. Konoplev, and I. Kulikova. Distributed Sensory System of Surface Cracks Monitoring Based on Electrical Impedance Tomography. *Electronics*, 7(8):131, 2018. doi: 10.3390/electronics7080131.

A. K. Saibaba, E. L. Miller, and P. K. Kitandis. A fast Kalman filter for time-lapse electrical resistivity tomography. *2014 IEEE Geoscience and Remote Sensing Symposium*, 2014. doi: 10.1109/IGARSS.2014.6947146.

Samorè, A. and Guermandi, M. and Placati, S. and Guerrieri, R. Parametric Detection and Classification of Compact Conductivity Contrasts With Electrical Impedance Tomography. *IEEE Transactions on Instrumentation and Measurement*, 66(10):2666–2679, 2017. doi: 10.1109/TIM.2017.2711818.

E. Santos and F. Simini. Electrical Impedance Tomography for pulmonary oedema extent monitoring: review and updated design. *Journal of Physics: Conference Series*, 407, 2012. doi: 10.1088/1742-6596/407/1/012024.

I. Sapuan, K. Ain, and A. Suryanto. Dual frequency electrical impedance tomography to obtain functional image. *Journal of Physics: Conference Series*, 853(012002), 2017. doi: 10.1088/1742-6596/853/1/012002.

I. Sapuan, M. Yasin, K. Ain, and R. Apsari. Anomaly Detection Using Electric Impedance Tomography Based on Real and Imaginary Images. *Sensors*, 20, 1907, 2020. doi: 10.3390/s20071907.

M. Serena Chiriaco, P. Ilaria, S. Fausto, P. Palmiro, and P. Elisabetta. mpedance sensing platform for detection of the food pathogen listeria monocytogenes. 7(347), 2018. doi: https://doi.org/10.3390/electronics7120347.

R. Seward, M. Ethan, M. Courtney, Z. Fu, G. Hilda, M. Badria, and H. Ryan. Using EIT to assess Pulmonary Function in ALS Patients. *In Proceedings of the 20th International Conference on Biomedical Applications of Electrical Impedance Tomography (EIT2019), London, UK*, 2019. doi: 10.5281/zenodo.2691705.

X. Shi, W. Li, F. You, X. Huo, C. Xu, Z. Ji, R. Liu, B. Liu, Y. Li, F. Fu, and X. Dong. High-Precision Electrical Impedance Tomography Data Acquisition System for Brain Imaging. *IEEE Sensors Journal*, 18(14):5974–5984, 2018. doi: 10.1109/JSEN.2018.2836336.

D. Silvera-Tawil, D. Rye, M. Soleimani, and M. Velonaki. Electrical Impedance Tomography

for Artificial Sensitive Robotic Skin: A Review. *IEEE Sensors Journal*, 15(4):2001–2016, 2015. doi: 10.1109/jsen.2014.2375346.

H. Sohal, H. Wi, A. L. McEwan, E. J. Woo, and T. I. Oh. Electrical impedance imaging system using FPGAs for flexibility and interoperability. *Biomed Eng Online*, 13:126, 2014. doi: 10.1186/1475-925X-13-126.

R. W. Stacey. *Electrical Impedance Tomography, SGP-TR-182*, chapter Recent developments in applied potential tomography-APT, pages 1–5. Stanford University, 1986.

Q. Wang, F. Li, J. Wang, X. Duan, and X. Li. Towards a Combination of Low Rank and Sparsity in EIT Imaging. *IEEE Access*, 7:156054–156064, 2019. doi: 10.1109/ACCESS.2019.2947439.

Y. Wang, S. Ren, and F. Dong. Focusing Sensor Design for Open Electrical Impedance Tomography Based on Shape Conformal Transformation. *Sensors*, 19(9):2060, 2019. doi: 10.3390/s19092060.

Y. Wei and F. Gao. Architecture design method for Structural Health Monitoring System(SHM) of Civil Aircraft. *2017 International Conference on Sensing, Diagnostics, Prognostics, and Control*, 2017. doi: DOI10.1109/SDPC.2017.144.

E. Widodo Aris. Design of low-cost and high-speed portable two-dimensional electrical impedance tomography (EIT). *International Journal of Engineering & Technology*, 7(2018):6458–6463, 2018. doi: 10.14419/ijet.v7i4.23298.

Y. Wu, D. Jiang, A. Bardill, S. de Gelidi, R. Bayford, and A. Demosthenous. A High Frame Rate Wearable EIT System Using Active Electrode ASICs for Lung Respiration and Heart Rate Monitoring. *IEEE Transactions on Circuits and Systems I: Regular Papers*, 65(11):3810–3820, Nov 2018. doi: 10.1109/TCSI.2018.2858148.

Y. Wu, D. Jiang, X. Liu, R. Bayford, and A. Demosthenous. A Human-Machine Interface Using Electrical Impedance Tomography for Hand Prosthesis Control. *IEEE Transactions on Biomedical Circuits and Systems*, 12(6), 2018. doi: 10.1109/TBCAS.2018.2878395.

Y. Wu, D. Jiang, A. Bardill, R. Bayford, and A. Demosthenous. A 122 FPS, 1 MHz Bandwidth Multi-Frequency Wearable EIT Belt Featuring Novel Active Electrode Architecture

for Neonatal Thorax Vital Sign Monitoring. *IEEE Transactions on Biomedical Circuits and Systems*, 13(5):927–937, 2019. doi: 10.1109/TBCAS.2019.2925713.

G. L. Zeng, editor. *Medical image reconstruction, a conceptual tutorial*. Cham (CH) Springer, 2009.

K. Zhang, M. Li, F. Yang, S. Xu, and A. Abubakar. Three-dimensional electrical impedance tomography with multiplicative regularization. *IEEE Trans Biomed Eng*, 66(9):2470–2480, 2019. doi: 10.1109/TBME.2018.2890410.

X. Zhang, Z. Li, and S. Zhu. A Novel Electrical Resistance Tomography System of Carbon Fiber Smart Layer for Structural Health Monitoring. *2009 IEEE International Conference on Intelligent Computing and Intelligent Systems*, 2009. doi: 10.1109/ICICISYS.2009.5357724.

D. Zuras, M. Cowlishaw, A. Aiken, M. Applegate, D. Bailey, S. Bass, D. Bhandarkar, M. Bhat, D. Bindel, S. Boldo, et al. IEEE standard for floating-point arithmetic. *IEEE Std 754-2008*, pages 1–70, 2008. doi: 10.1109/IEEESTD.2008.4610935.